Article - Discoveries

Genomic architecture controls spatial structuring in Amazonian birds

Gregory Thom[1*], Lucas Rocha Moreira[2,3], Romina Batista[4,5], Marcelo Gehara[6], Alexandre Aleixo[7,8], Brian Tilston Smith[1]

[1]Department of Ornithology, American Museum of Natural History, New York, United States.

[2]Program in Bioinformatics and Integrative Biology, University of Massachusetts Chan Medical School, Worcester, MA, USA.

[3]Broad Institute of MIT and Harvard, Cambridge, MA, USA.

[4]Instituto Nacional de Pesquisas da Amazônia, Manaus, Brazil.

[5]Gothenburg Global Biodiversity Centre, Gothenburg, Sweden.

[6]Department of Earth and Environmental Sciences, Rutgers University, Newark, United States.

[7] Finnish Museum of Natural History, University of Helsinki, Helsinki, Finland.

[8] Instituto Tecnológico Vale, Belém, Brazil.

[*]Corresponding author: gthomesilva@amnh.org

Abstract

Large rivers are ubiquitously invoked to explain the distributional limits and speciation of the Amazon Basin's mega-diversity. However, inferences on the spatial and temporal origins of Amazonian species have narrowly focused on evolutionary neutral models, ignoring the potential role of natural selection and intrinsic genomic processes known to produce heterogeneity in

differentiation across the genome. To test how these factors may influence evolutionary inferences across multiple taxa, we sequenced whole genomes of populations for three bird species that co-occur in southeastern Amazonian and exhibit different life histories linked to their propensity to maintain gene flow across the landscape. We found that phylogenetic relationships within species and demographic parameters varied across the genome in predictable ways. Genetic diversity was positively associated with recombination rate and negatively associated with the species tree topology weight. Gene flow was less pervasive in regions of low recombination, making these windows more suitable for commonly used phylogenetic methods that assume a bifurcating-branching model. To corroborate that these associations were attributable to selection, we modeled the signature of adaptive alleles across the genome taking demographic history into account, and found that on average 31.6 % of the genome showed high probability for patterns consistent with selective sweeps and linked selection directly affecting the estimation of evolutionary parameters. By implementing a comparative genomic approach we were able to disentangle the effects of intrinsic genomic characteristics and selection from the neutral processes and show how speciation hypotheses are sensitive to genomic architecture.

Introduction

Across the Amazon Basin, large rivers delimit the distribution of hundreds of rainforest taxa (Cracraft 1985; Bates et al. 1998; da Silva et al. 2005). The spatial patterns that underlie these distributions have been central for understanding how diversity originates in the hyperdiverse Neotropics (Haffer 1969; Haffer 2008; Ribas et al. 2012; Smith et al. 2014; Silva et al. 2019). The species isolated by large rivers show complex and highly variable relationships that span millions of years, with limited congruence in spatial patterns of diversification and

historical demography (Smith et al. 2014; Silva et al. 2019). Reduced genomic approaches have revealed that factors such as gene flow may hinder inferences on the origins of species distributed across Amazonian rivers (Weir et al. 2015; Barrera-Guzmán et al. 2018; Ferreira et al. 2018; Berv et al. 2021; Del-Rio et al. 2021; Luna et al. 2021; Musher et al. 2021). In addition to gene flow, intrinsic (e.g., recombination rate) and extrinsic (e.g., selection) processes that influence the landscape of genomic diversity and differentiation may further obfuscate biogeographic inferences by affecting the estimation of phylogenetic and demographic parameters (Li et al. 2019; Martin et al. 2019; Johri 2021). Elucidating the relationships between the processes driving genomic evolution may yield more accurate inferences on the spatial and temporal history of species, providing a new perspective into the hotly debated origins of Amazonian biodiversity.

The genomic landscape of genetic diversity is ubiquitous across taxonomic groups indicating that evolutionary signal is dependent on which portions of the genome are examined (Delmore et al. 2018; Li et al. 2019; Martin et al. 2019; Manthey et al. 2021; Johri et al. 2021). Components of genomic architecture, such as chromosome inheritance, meiotic recombination, the density of targets of selection, biased gene conversion, and mutation rate operate simultaneously and heterogeneously across the genome, resulting in highly variable levels of genetic diversity and divergence at both intra- and interspecific scales (Meunier and Duret 2004; Garrigan et al. 2012; Cruickshank and Hahn 2014; Roux et al. 2014; Seehausen et al. 2014; Fontaine et al. 2015; Wolf and Ellegren 2017; Smith et al. 2018; Edelman et al. 2019; Martin et al. 2019; Johri et al.). For instance, recent evidence indicates that phylogenetic signal (e.g., the support for a particular topology) is associated with chromosome size and recombination rate, with larger chromosomes having slower rates that yield higher support for inferred species trees

(Martin et al. 2019). However, most methods used in phylogenomics do not account for the multiple processes that shape the genomic landscape, which may confound estimation of evolutionary histories (Ewing and Jensen 2016; Schrider et al. 2016; Li et al. 2019). This is critical given that modern biogeography relies heavily on phylogenetic and population genetic approaches to explore the spatial history and demography of populations (Knowles 2009; Edwards et al. 2021). Understanding how genomic architecture may affect inferences of spatial diversification histories will provide a clearer picture on the relative roles of intrinsic genomic characteristics, natural selection, and neutral processes on speciation (Pouyet et al. 2018; Johri et al. 2020).

Linked selection can have a large impact on genome-wide variation, but its effects on phylogenetic signal and demographic history of species are only starting to be explored (Li et al. 2019; Martin et al. 2019). The indirect influence of positive and background selection on linked neutral sites can reduce genetic diversity around target regions, decreasing local effective population size (*Ne*) and leading to faster fixation of alleles (Charlesworth 1998; Cruickshank and Hahn 2014; Burri et al. 2015). The intensity of linked selection on neutral sites is predicted by the interplay between the local density of targets under selection and the recombination rate, with more pronounced reductions in genetic diversity occurring in genomic regions with stronger selection and lower recombination (Smith and Haigh 1974; Charlesworth et al. 1993; Hudson and Kaplan 1995; Gillespie 2000; Zeng 2013). Areas of low recombination should also be more resistant to the confounding effects of gene flow and function as hotspots of phylogenetic signal (Martin et al. 2019; Chase et al. 2021). In these regions, linkage is maintained between introgressed variants and large genomic blocks may be removed from the population if deleterious alleles are present (Brandvain et al. 2014; Schumer et al. 2018; Mořkovský et al.

2018). The reduced impact of gene flow in regions of low recombination indicates that the phylogenetic signal is more likely to follow a bifurcating tree model, fitting the assumptions of most phylogenetic methods (Li et al. 2019; Martin et al. 2019). However, linked selection on low recombination areas violates neutral models of evolution and affects genome-wide estimations of demographic parameters (Schrider et al. 2016; Johri et al. 2020). A growing number of studies have reported associations between recombination, levels of genetic diversity, and phylogenetic relationships, both within and between chromosomes (Cutter and Payseur 2013; Burri et al. 2015; Dutoit, Burri, et al. 2017; Tigano et al. 2021).

Although recent studies show that linked selection impacts a larger proportion of the genome than previously thought (Kern and Hahn 2018; Pouyet et al. 2018), the degree of this impact varies between species (Jensen et al. 2019; Tigano et al. 2021). For instance, the divergence between populations with high rates of gene flow might be restricted to small areas of the genome, maintained by strong divergent selection whereas the vast majority of the genome might show reduced differentiation due to widespread introgression (Ellegren et al. 2012). In contrast, genomic differentiation in allopatric populations, or under reduced levels of gene flow, tends to be more widespread, given the higher contribution of genetic drift sorting alleles in isolated populations. This latter scenario should produce a stronger association between genomic architecture and levels of genetic differentiation across the genome.

In this study, we model the impact of genomic architecture on patterns of genetic diversity and spatial differentiation of three bird species that co-occur in southeastern Amazonian. These taxa have different propensities to move across space that are linked to their life histories, resulting in landscapes of genomic differentiation impacted by distinct levels of gene flow. We hypothesize that if linked selection led to congruent patterns of genetic diversity

across the genome, then metrics associated with species differentiation and genetic diversity should be correlated with recombination rate, the density of targets under selection, and chromosome size. Alternatively, species could have idiosyncratic patterns of association with genomic architecture, driven by other factors such as historical demography and the level of differentiation across rivers. We demonstrate that the interplay between recombination, selection, and gene flow lead to a highly variable landscape of genetic diversity and differentiation within and between species, and impact biogeographic inference under different population histories.

Results

Population genetics summary statistics and genomic features vary between species and across the genome

We generated 95 whole-genome sequences for three species of birds, *Phlegopsis nigromaculata* (n=31), *Xiphorhynchus spixii* (n=31), and *Lipaugus vociferans* (n=26) that are co-distributed across three Amazonian areas of endemism, the Tapajos, Xingu, and Belem (Figure 1; Table S1). We recovered a mean coverage of 10x across all species. On average, 88% of the pseudo-chromosome reference genomes were recovered with coverage above 5x per individual (Table S1). Benchmarking Universal Single-Copy Orthologs analyses performed in BUSCO v2.0.1 (Waterhouse et al. 2018) identified a high proportion of targeted genes on the references used for *P. nigromaculata* (89.3%), *X. spixii* (89.1%), and *L. vociferans* (93.4%; Table S2). The number of segregating sites were of a similar magnitude but varied: *P. nigromaculata* (n = 20,838,931), *X. spixii* (n = 26,583,784), and *L. vociferans* (n = 21,769,167). The proportion of missing sites per individual was on average 18% (Table S1). Summary statistics estimated from 100kb non-overlapping sliding windows and mean values per chromosome showed that levels of

genetic diversity varied substantially across species and within and between chromosomes (Figure 2). Populations from species with higher putative dispersal abilities (*L. vociferans* and *X. spixii*) had substantially more nucleotide diversity (Figure 3; Tables S3-S5). We observed higher nucleotide diversity on smaller chromosomes in *P. nigromaculata* (Pearson's correlation R = -0.6; p-value = 0.002; n = 26) and *X. spixii* (Pearson's correlation R = -0.36; p-value 0.047; n = 32) but not in *L. vociferans* (Pearson's correlation R = -0.01; p-value = 0.94 ; n = 32; Figure S1-S6; Table S6-S11). We also found similar associations with *Dxy*, number of segregation sites, and Tajima's D (Figure S1-S6; Table S6-S11). These results support a highly heterogeneous landscape of genetic diversity across the genome of the three studied species.

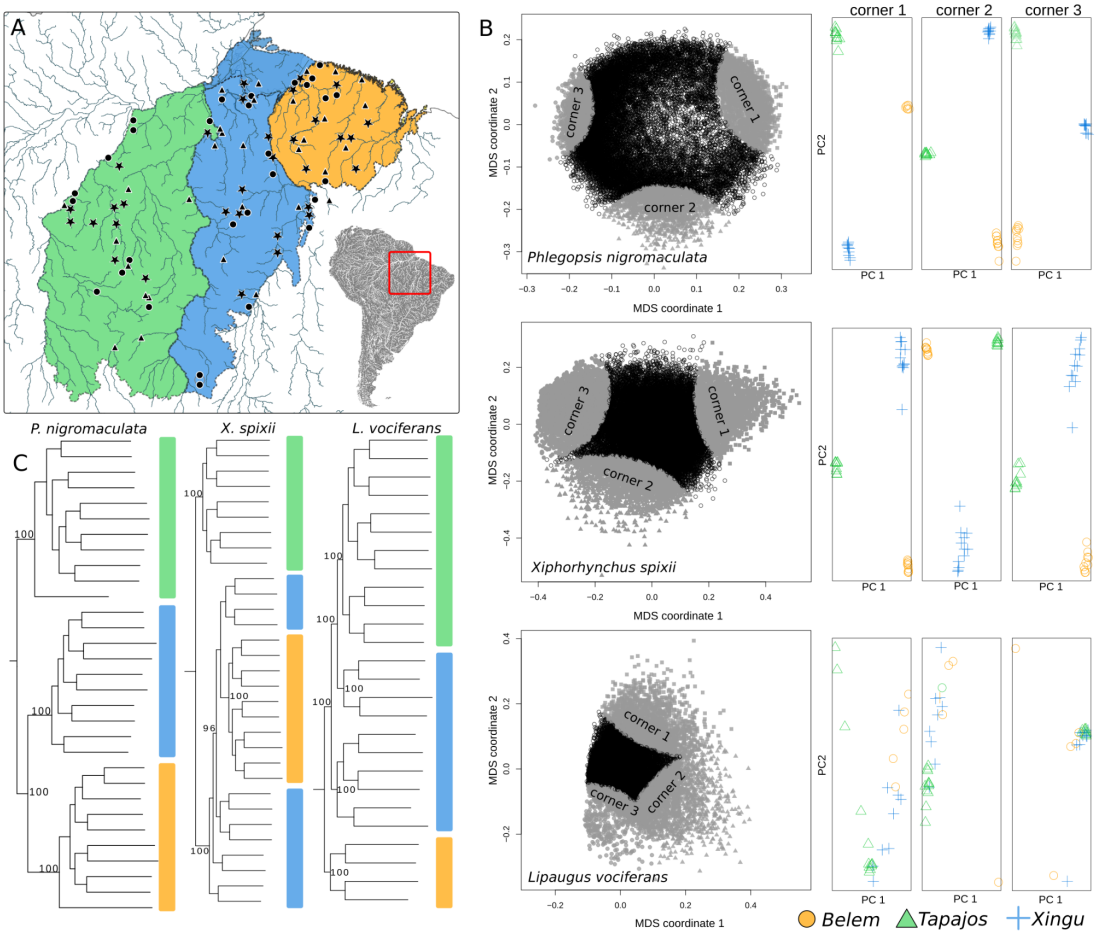

150 **Figure 1:** Contrasting patterns of genomic differentiation and spatial relationships between
151 populations of three species of birds occurring in southeastern Amazonia. Geographic
152 distribution of genomic samples for each species **(A)**. Triangles, stars, and circles are sampled
153 localities for *Phlegopsis nigromaculata*, *Xiphorhynchus spixii*, and *Lipaugus vociferans*,
154 respectively. Each colored polygon in the map represents a major Amazonian interfluve (area of
155 endemism): Tapajos (Green), Xingu (Blue), and Belem (Yellow). **(B)** Patterns of genetic
156 structure across the genome were obtained with local PCAs based on 10kb windows. Left: plots
157 for the first and second multidimensional coordinates, where each point represents a genomic
158 window. Gray points represent corners clustering the 10% of the windows closer to the three
159 further points in the graph. Right: PCA plots for the first and second principal components,
160 combining the windows of each corner. **(C)** Supermatrix phylogenetic estimations based on
161 concatenated SNPs. Numbers on the nodes represent bootstrap support for major nodes in the
162 tree. Color bars next to terminals represent geographic location following the map (A).
163

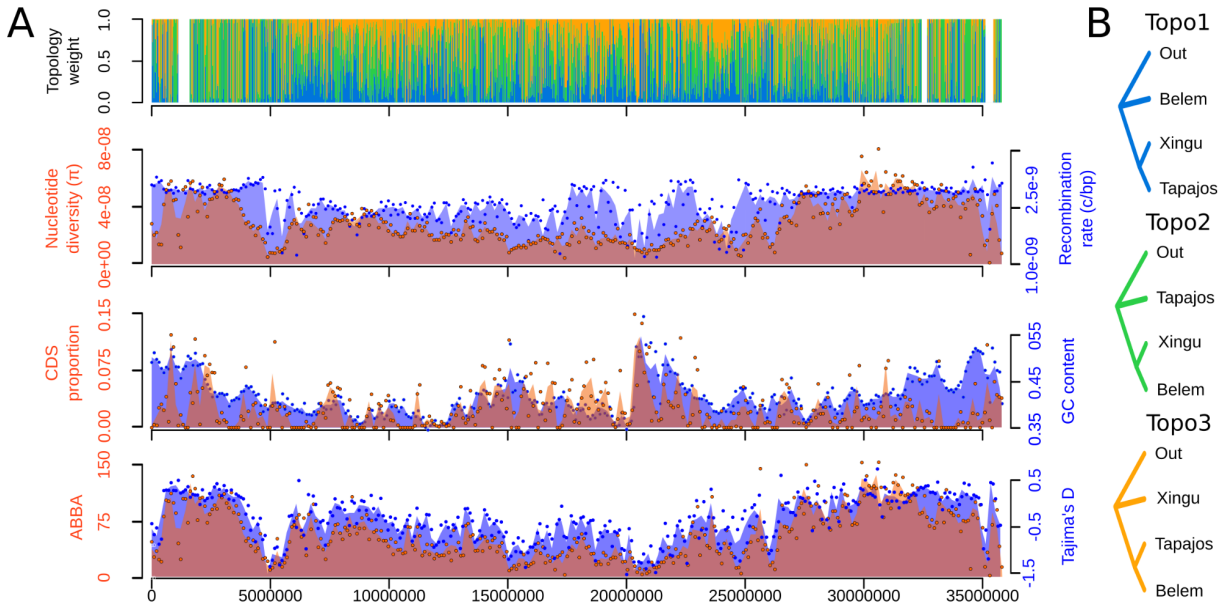

164

165 **Figure 2:** Phylogenetic signal for the species tree was higher on central portions of

chromosomes and was associated with genomic architecture. **(A)** Example of how phylogenetic signal and summary statistics are distributed across a chromosome. Shown are pseudo-chromosome 6 of *P. nigromaculata*. On the top graph, colored bars represent the weight for the three alternative topologies shown in **(B)** for the relationship between Tapajos, Belem, and Xingu areas of endemism. On the three bottom graphs, the magenta color represents the overlap between the orange (y-axis on the left) and blue (y-axis on the right) tones. Estimates of nucleotide diversity, recombination rate, and Tajima's D were based on the Tapajos population. ABBA represents the number of sites supporting Topology 2 assuming Topology 1 as the species tree.

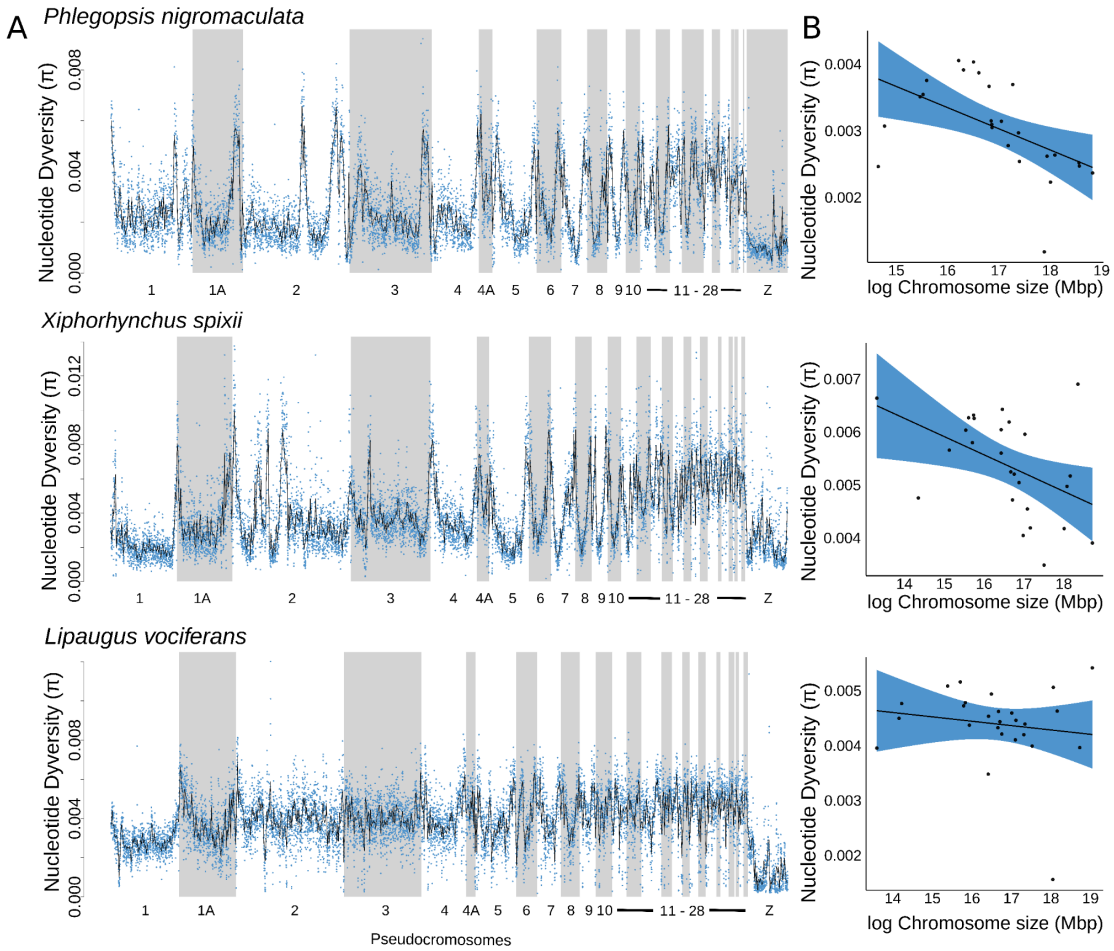

Figure 3: Nucleotide diversity varied within and between pseudo-chromosomes and across

177 species. **(A)** Distribution of nucleotide diversity (π) across chromosomes for the three studied
178 species. **(B)** Scatterplot and regression line with 95% confidence interval models with average
179 nucleotide diversity as a function of chromosome size. *Phlegopsis nigromaculata* - Pearson's
180 correlation R = -0.6; p-value = 0.002; n = 26; *Xiphorhynchus spixii* - Pearson's correlation R = -
181 0.36; p-value 0.047; n = 32; *Lipaugus vociferans* - Pearson's correlation R = -0.01; p-
182 value=0.94 ; n = 32.

183 We found that genomic regions with a reduced meiotic recombination rate were less
184 impacted by gene flow, and had stronger signatures of linked selection, with greater genetic
185 differentiation. To test for associations between recombination rate and genetic metrics while
186 accounting for historical demography, we estimated the per-base recombination rate (r) with
187 ReLERNN (Adrion et al. 2020). Recombination rate varied considerably across the genome of
188 *P. nigromaculata* (mean r = 2.103e-9; SD = 4.413e-10), *X. spixii* (mean r = 1.234e-9; SD =
189 7.190e-10), and *L. vociferans* (mean r = 1.776e-9; SD = 4.025e-10; Figure S7) but in predictable
190 ways. We found that regions with higher recombination rates were often in chromosome ends
191 (Figure S7) and smaller chromosomes (Figure S4-S6), and were positively correlated with gene
192 density and nucleotide diversity in all three species (Figure S8; Table S12). Loess models with
193 recombination rate and gene density as covariate predictors explained a large proportion of the
194 variation in genetic diversity in *P. nigromaculata* (R^2 = 0.33), *X. spixii* (R^2 = 0.65), and *L.*
195 *vociferans* (R^2 = 0.41; Figure S8, S9). These results suggest a significant effect of linked
196 selection driving genomic patterns of diversity.

197 Genome-wide levels of differentiation between species match the evolutionary
198 expectations associated with their life history. The least dispersive species that inhabit the
199 understory, *P. nigromaculata*, had the most pronounced levels of genetic structure across rivers,

followed by *X. spixii* which occupies the midstory, and the most dispersive, canopy species, *L. vociferans*, had the shallowest structure. To visualize patterns of genetic structure based on independently evolving sets of SNPs (linkage disequilibrium $R^2 < 0.2$), we used Principal Component Analysis (PCA). In *P. nigromaculata*, three isolated clusters of individuals supported strong geographic structure, consistent with previous studies based on mtDNA, spatially matching areas of endemism (Aleixo et al. 2009; Silva et al. 2019; Figure 1, S10). In *X. spixii*, the PCA supported strong differentiation between the Tapajos from Belem and Xingu populations, which had a substantial overlap in PC2 (5.0% of the explained variance; Figure S10). For *L. vociferans*, all samples clustered together, indicating a lack of spatial structure in the genetic variation (Figure S10). In agreement with these results, average *Fst* between populations was considerably higher in *P. nigromaculata* (mean *Fst* = 0.1262; SD = 0.09) than in *X. spixii* (mean *Fst* = 0.059; SD = 0.046, and *L. vociferans* (mean *Fst* = 0.008; SD = 0.019). Pairwise *Fst* between populations was, in general, negatively correlated with genetic diversity metrics in all three species, and it was negatively correlated with recombination rate in *P. nigromaculata* and *X. spixii* (Figure S1-S6; Table S6-S11).

Levels of genetic structure varied substantially across the genome, indicating that the support for alternative spatial patterns of differentiation was directly associated with intrinsic genomic processes. To explore the genome-wide variation in genetic structure, we used local PCAs across sliding windows using lostruct v0.0.0.9 (Li and Ralph 2019). Local PCAs showed that distinct parts of the genome support different clustering patterns in *P. nigromaculata* and *X. spixii*, likely reflecting distinct evolutionary relationships between populations (Figure 1). In *L. vociferans*, we observed a gradient between Tapajos, Xingu, and Belem individuals, without clear structuring, consistent with the low *Fst* estimates reported for this species (Figure 1).

Genetic structure, as described by the first two MDS axes obtained with lostruct, was associated with recombination in *P. nigromaculata* (MDS1: R^2 = -0.04, p-value < 0.0001, n = 20,143 windows) and *X spixii* (MDS1: R^2 = 0.017, p-value < 0.0001, n = 28,803 windows; MDS2: R^2 = -0.15, p-value < 0.0001, n = 28,803 windows) but not in *L. vociferans* (R^2 < 0.001 for all MDSs, n = 25,007 windows), indicating that for the species with marked genetic structure across rivers, recombination was a key predictor of spatial differentiation. These results highlight the high variation in patterns of genetic structure across the genome as well as the contrast between patterns of diversification of sympatric species distributed across Amazonian rivers.

Although the association between recombination rate and genetic diversity supports the effect of linked selection, it does not indicate which portions of the genome are directly impacted by this process. To further explore the extent of linked selection across the genome, we used a machine learning approach implemented on diploS/HIC (Kern and Schrider 2018) to predict which 20kb genomic windows were evolving under neutrality or had signatures of selective sweeps and linked selection (i.e., background selection; Charlesworth et al. 1993). We initially simulated genomic windows under distinct selective regimes accounting for historical oscillations in effective population size and uncertainty in demographic parameters using discoal (Kern and Schrider 2016). To account for the historical demography of the analyzed populations we estimated population size changes occurring in the last 300,000 years with SMC++ (Terhorst et al. 2017) and included these estimates in the discoal simulations (Figure S11). The convolutional neural network used in this approach produced an average accuracy for model classification of 0.69 and a false positive rate of 0.27 among species (Table S13). In all three species, a significant proportion of the genome was estimated to have signatures of selective sweeps or linked selection (mean = 43.3%). In *P. nigromaculata*, 30.29% of tested windows had

246 a high probability (>0.70) for models including the direct or indirect effect of selection (Figure
247 4). For *X. spixii* (44.83%) and *L. vociferans* (54.77%), we obtained even higher proportions
248 (Figure 4). By accounting for the estimated false positive rate on average 31.6% of the genomes
249 we analyzed had signatures of selective sweeps or linked selection.

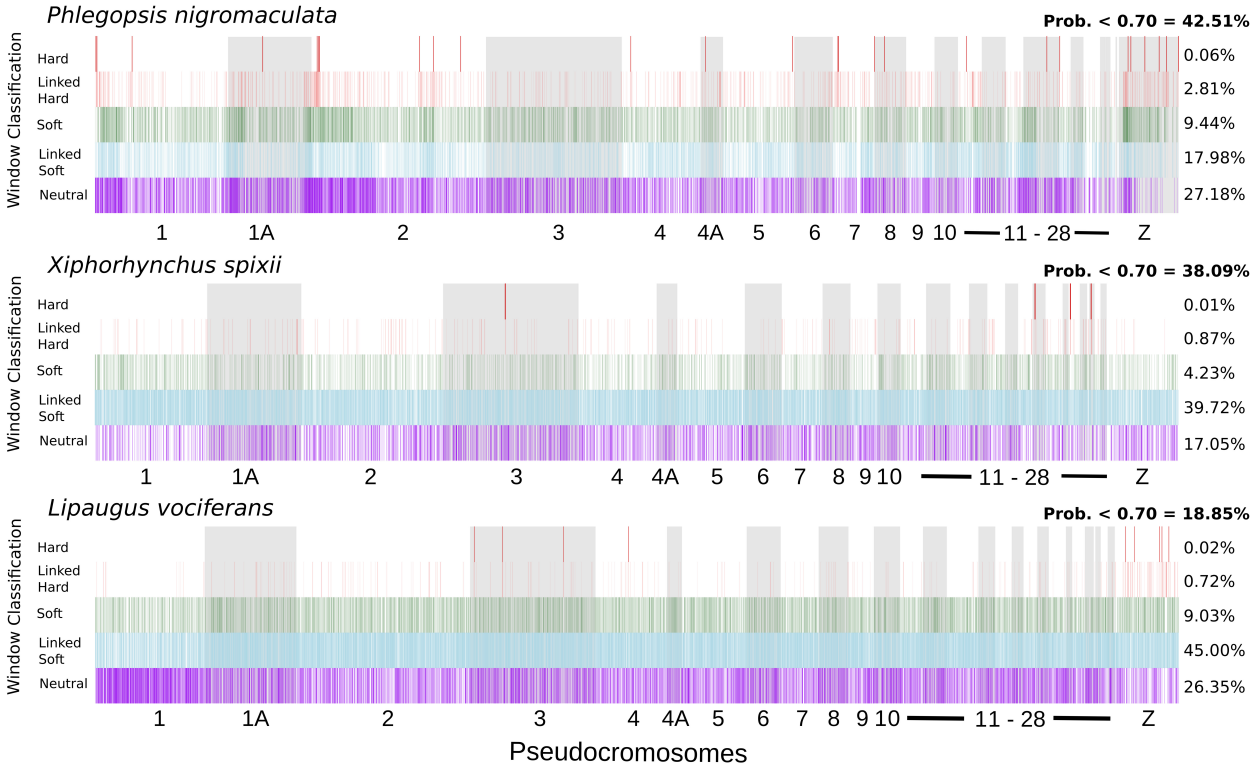

250

251 **Figure 4:** Signature of selection across the genomes of the studied species. Vertical bars
252 represent the model with the highest probability for 20 kb genomic windows. On the right is the
253 percentage of windows assigned to each of the five models with high probability (>0.70): hard
254 sweep, linked to hard sweep, soft sweep, linked to soft sweep, and neutral. In Bold is the
255 proportion of windows with low probability for model classification.

256

257 *Phylogenetic signal was associated with genomic architecture.*

258 We explored how evolutionary relationships were distributed across the genome of the

co-occurring species to test which aspects of the genomic architecture best predicted phylogenetic signal. First, we estimated topologies for each species in IQTREE-2 v2.1.5 (Nguyen et al. 2015) by concatenating SNPs and controlling for ascertainment bias (Figure 1). We found substantial variation in topology between species, with clades matching the three areas of endemism only in *P. nigromaculata.* In *X. spixii*, Belem individuals were nested within Xingu despite forming a monophyletic group. In *L. vociferans*, the clustering of individuals matched their spatial distribution.

The support for alternative species tree topologies varied with recombination rate and genetic diversity (Figure 5). To explore how phylogenetic relationships varied with genomic characteristics and population genetics summary statistics, we estimated gene trees for non-overlapping genomic windows and calculated species trees for subsets of the genome. For *P. nigromaculata* we did not obtain high support for any topology when estimating the species tree from genome-wide loci, but the topology with the highest probability (posterior probability = 0.81) matched the concatenated SNP tree (Figure 5). The topology estimated from genomic regions with high recombination matched the concatenated tree, but regions of low recombination placed Tapajos and Xingu as sisters (Figure 5). A similar pattern was observed when filtering gene trees based on π and *Dxy*. The phylogenetic signal in *X. spixii* and *L. vociferans* were more stable, with widespread support for the same topology across the genome but with substantially higher weight for that topology in areas with lower recombination and lower genetic diversity. Phylogenetic signal also co-varied with chromosome size in *P. nigromaculata* but not in *X. spixii* and *L. vociferans*. In *P. nigromaculata*, macro chromosomes supported the topology found in low recombination areas (Topology 1), while microchromosomes (<50MB) supported the concatenated tree (Topology 2; S12-S14). Our

282 results suggest that support for the species tree was higher in regions with reduced diversity and
283 recombination rates.

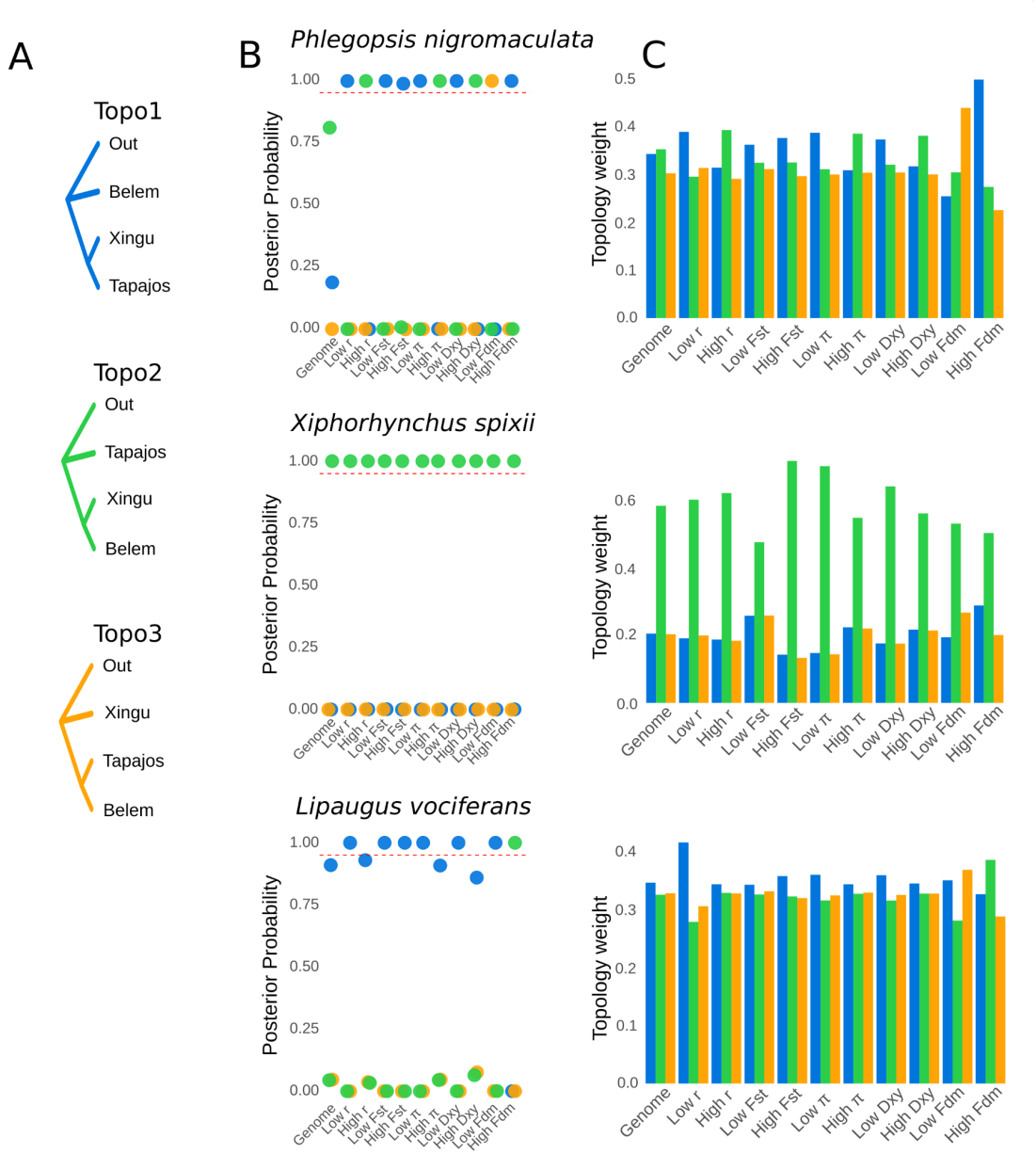

284

285 **Figure 5:** Species tree and topology weights vary accordingly to recombination rate and genetic
286 diversity. **(A)** Alternative topologies for the relationship between the three areas of endemism
287 and the outgroup; **(B)** posterior probabilities for the three topologies for windows across the
288 whole-genome and for distinct subsets of genomic windows that were selected based on upper

and lower thresholds for summary statistics; and **(C)** weights for three topologies for windows across the whole-genome and for distinct subsets of genomic windows that were selected based on upper and lower thresholds for summary statistics. *r* - Recombination rate; *Fst* - Fixation index; *π* - Nucleotide diversity; *Dxy* - Genetic distance; *Fdm* - Introgression proportion.

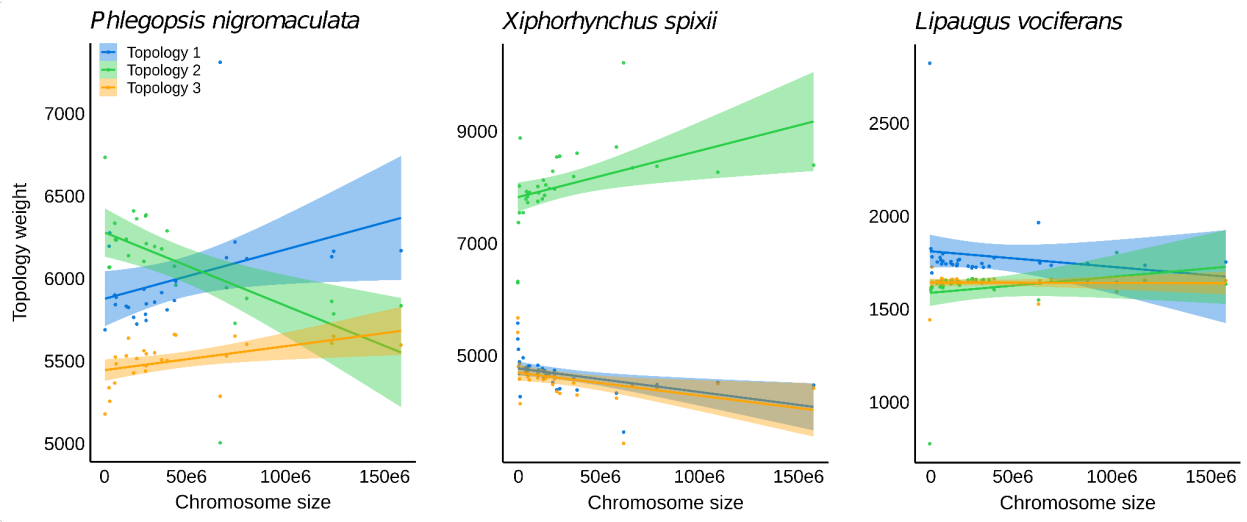

Figure 6: Chromosome size was associated with topology weight across the genome of *Phlegopsis nigromaculata* (Topology 2 - $R^2 = 0.31$, p-value = 0.003; Topologies 1 and 2 p-value > 0.05, n= 26) but not in *Xiphorhynchus spixii* (p-value > 0.05 for all three topologies, n = 32) , and *L. vociferans* (p-value > 0.05 for all three topologies, n = 32). Scatterplot and regression line with 95% confidence interval showing the relationship between topology weights and chromosome size. We tested three alternative unrooted topologies for the relationship between the three areas of endemism (Tapajos, Xingu, and Belem): Topology 1 (outgroup, Belem (Xingu, Tapajos)), Topology 2 (outgroup, Tapajos (Xingu, Belem)), and Topology 3 (outgroup, Xingu (Belem, Tapajos)).

The weight for alternative topologies varied considerably across windows and was associated with genomic architecture. To test how the probability of alternative topologies varied

306 across the genome, we calculated topology weights using Twisst (Martin and Van Belleghem
307 2017) independently for each species. This analysis was performed on genomic windows with
308 100 SNPs and assumed the three possible unrooted trees representing the relationship between
309 the three areas of endemism plus an outgroup. From hereafter we refer to these three unrooted
310 topologies as Topology 1 (outgroup, Belem (Xingu, Tapajos)), Topology 2 (outgroup, Tapajos
311 (Xingu, Belem)), and Topology 3 (outgroup, Xingu (Belem, Tapajos)). When averaging weights
312 for genome-wide windows of *P. nigromaculata* we observed a higher weight for Topology 2,
313 followed closely by Topology 1. When considering distinct subsets of genomic windows based
314 on upper and lower thresholds for summary statistics, for *P. nigromaculata*, there was substantial
315 variation in which topology had the highest average weight, consistent with our species tree
316 approach (Figure 5). For the other two species, we found less variation along the genome for the
317 topology with the highest average weight. The topology with the highest weight also varied
318 across chromosomes of different sizes. In *P. nigromaculata*, smaller chromosomes had a higher
319 weight for Topology 2, putatively derived from gene flow (Figure 6). In *X. spixii* we observed a
320 progressive increase in the weight for the species tree (Topology 2) in larger chromosomes,
321 despite a non-significant correlation. In *L. vociferans* all three topologies had a similar weight
322 across chromosomes. In summary, these results reinforced the view that intrinsic genomic
323 features directly shape the distribution of the phylogenetic signal.

324 The conflicting phylogenetic pattern observed for *P. nigromaculata* could be driven by
325 gene flow increasing the signal for the topology where introgressing populations are sisters. To
326 explore how topology weight varied according to gene flow and intralocus recombination, we
327 performed coalescent simulations with demographic parameters similar to those estimated for *P.*
328 *nigromaculata,* and we calculated topology weights using the approach mentioned above. Our

329 simulations suggested that in the absence of gene flow, the frequency of alternative topologies
330 was similar (Figure S15). The presence of gene flow between non-sister species produces a
331 deviation from this pattern, increasing the average weight for the topology with introgressing
332 populations as sisters. This relationship was further intensified by intralocus recombination
333 (Figure S15). Although our simulations corroborate that recombination rate by itself does not
334 affect levels of genetic diversity (Hudson 1983), it does affect levels of ILS between populations,
335 particularly when gene flow was present by increasing the variance of topology weights across
336 the genome (Figure S15). When comparing the results obtained with this simulation approach
337 with the genome-wide topology weights obtained for *P. nigromaculata,* our results suggest that
338 gene flow between non-sister taxa was likely increasing the weights for one of the two best
339 topologies.
340
341 *Gene flow affected phylogenetic inference*
342 When modeling gene flow, our results indicated that the topology recovered for low
343 recombination areas was the best genome-wide tree. To estimate the probability for alternative
344 topologies and demographic parameters for the entire genome explicitly accounting for gene
345 flow we used a multiclass neural network approach with Keras v2.3
346 (https://github.com/rstudio/keras) in R. We simulated genetic data under the three possible
347 unrooted topologies for the relationship between areas of endemism using uniform priors for *Ne*,
348 gene flow between geographically adjacent populations, and divergence times. We selected one
349 10kb window every 100kb to reduce the effect of linkage between windows, excluding windows
350 with missing data. This procedure yielded a total of 7,213, 9,140, and 9,693 windows for *P.*
351 *nigromaculata, X. spixii,* and *L. vociferans,* respectively. Finally, we randomly selected 5,000

windows per species. Genomic windows were converted into feature vectors representing the mean and variance of commonly used population genetics summary statistics. On average, this approach produced highly accurate model classification probabilities (neural network accuracy = 0.93; categorical cross-entropy = 0.17) and a high correlation between observed and estimated parameters for testing data sets with low mean absolute errors (Table S14-S16). PCAs and goodness-of-fit analyses showed that simulated models matched observed values of summary statistics. In *P. nigromaculata,* we obtained a high probability for Topology 1 (probability = 0.86), conflicting with the concatenated and species tree topology (Topology 2; probability = 0.12) but agreeing with the topology of low recombination areas (Table S17). Divergence times were highly variable between species. In *P. nigromaculata* the initial divergence between Belem and the ancestor of the Tapajos and Xingu lineages, diverged at 149,836ya (SD = 15,272; MAE = 36,576; Table S14), followed by the divergence between the later populations at 77,866ya (SD = 17,849; MAE = 37,810). In *X. spixii* (Topology 2; probability = 0.99), the first divergence event was estimated at 218,858ya (SD = 12,095; MAE = 30,668), followed by a more recent divergence event at 40,303ya (SD = 16,236; MAE = 32,798; Table S15). For *L. vociferans* (Topology 1; probability = 0.54) divergence times were the most recent, occurring within the last 40,000 years, reflecting the lack of population structure in this species (Table S16). Our data indicated that gene flow among *P. nigromaculata* populations (2Nm) was negligible between Tapajos and Xingu (migration between Tapajos and Xingu = 0.002; SD = 0.005; MAE = 0.161) and low between the non-sisters in Xingu and Belem (migration between Xingu and Belem = 0.484; SD = 0.486; MAE = 0.138; Table S14). In *X. spixii*, we inferred moderate rates of gene flow between populations, which was highest between the recently diverged Xingu and Belem populations (migration between Xingu and Belem = 2.075; SD = 0.144; MAE = 0.139; Table

S15). In *L. vociferans* we also estimated moderate to high gene flow among populations (migration between Tapajos and Xingu = 2.347; MAE = 0.175; migration between Xingu and Belem = 1.827; MAE = 0.205; Table S16). Although the phylogenetic conflict found in *P. nigromaculata* was attributed to introgression, we found relatively reduced levels of gene flow between populations, indicating that ancestral gene flow might be the source of the conflict.

Selection biases estimates of demographic parameters

Given the considerable proportion of the genome with signatures of selective sweeps and background selection in all three species, we explored how selection might impact estimates of demographic parameters. We estimated parameters from subsets of genomic windows classified under distinct selection regimes with diploS/HIC using our machine learning approach. We selected up to 1,000 windows assigned to each of the five models tested in diploS/HIC with a probability > 0.70, and estimated demographic parameters based on the topology with the highest probability considering all genomic windows (Topology 1 for *P. nigromaculata* and *L. vociferans*, and Topology 2 for *X. spixii*). We found that genome-wide windows yielded more similar estimates for *Ne* and gene flow from regions inferred to be subject to selection than neutral regions (Figure 7). Our approach supported higher *Ne* and gene flow in neutral areas of the genome than areas under selection with little to no overlap of standard error distributions (Figure 7).

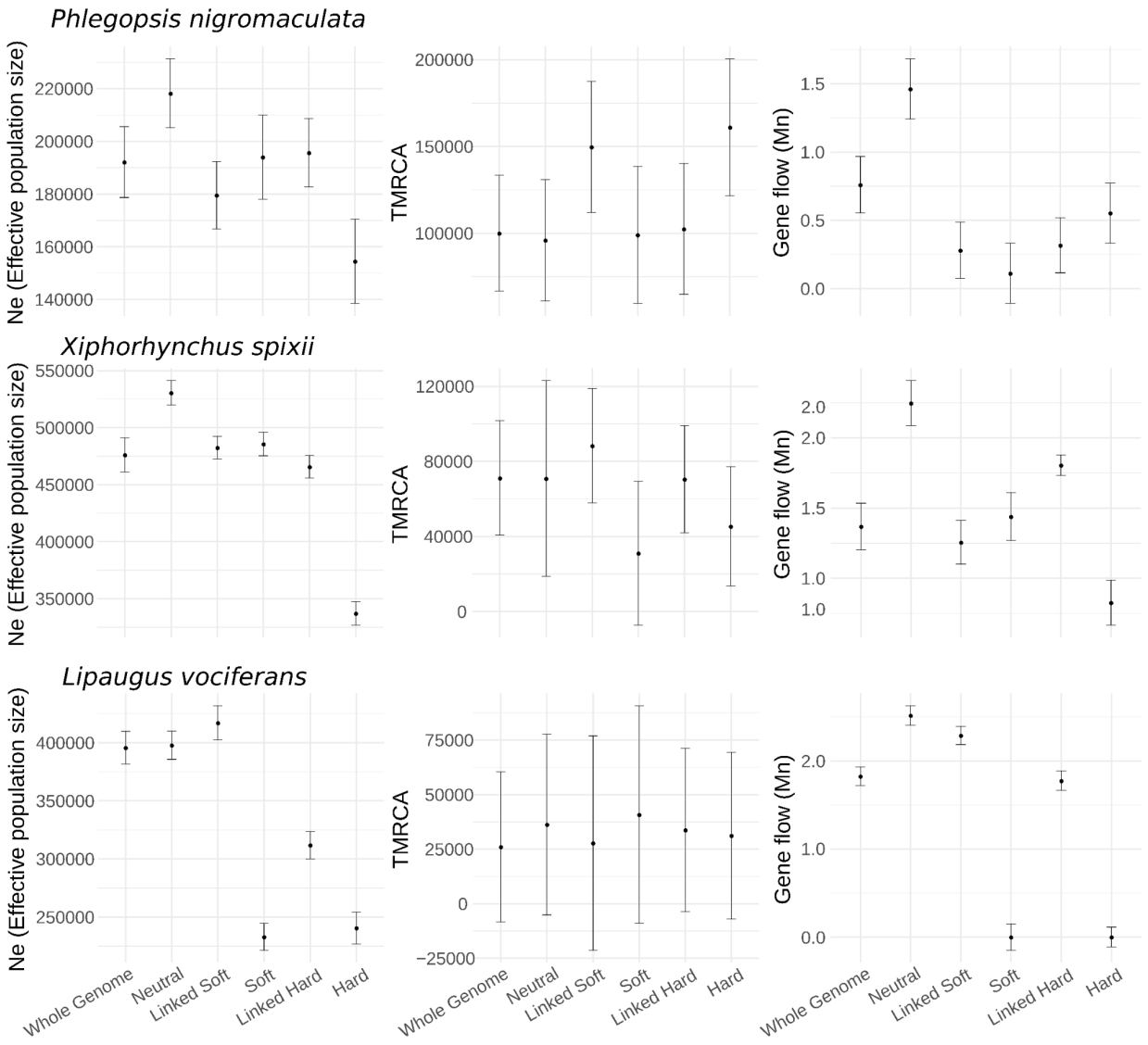

Figure 7: Genomic regions inferred to be evolving neutrally had larger effective population sizes and higher gene flow than areas with signatures of selection. Demographic parameter estimation for the three studied species of Amazonian Birds. *Ne* - Effective population size of the Tapajos population. TMRCA - Time to the most recent common ancestor of the most recent divergence event; Gene flow - Gene flow rate between Tapajos and Xingu populations. Classes on the x-axis represent genome-wide windows (Whole Genome), and subsets of genomic windows assigned with high probability to distinct models tested with diploS/HIC. Neutral - neutrally evolving windows; Linked Soft - windows linked to a soft sweep; Soft - windows assigned to a soft

403 sweep; Linked Hard - windows linked to a hard sweep; Hard - windows assigned to a hard
404 sweep.
405
406 Demographic parameters varied considerably across the genome and were strongly
407 associated with the recombination rate (Figure S16; Table S18). To explore the associations
408 between demographic parameter estimation and genomic architecture, we calculated the
409 probability of alternative topologies and estimated demographic parameters for 100kb genomic
410 windows, taking into account intralocus recombination. To increase model classification
411 accuracy, we only tested the two most likely topologies based on the spatial distribution of the
412 populations. This approach yielded a high accuracy in model classification (accuracy = 0.9314;
413 categorical cross-entropy = 0.18). We also recovered high correlations between simulated and
414 pseudo observed data indicating good accuracy in parameter estimation for *Ne* (average R^2 =
415 0.94; average MAE = 73,099 individuals) and divergence times (average R^2 = 0.87; average
416 MAE = 39,172ya) but not for gene flow (average R^2 = 0.54; average MAE = 0.19 migrants per
417 generation). Effective population sizes and divergence times varied over one order of magnitude,
418 and gene flow over two orders of magnitude across the genome. The substantial variation in *Ne*
419 and gene flow across the genome was associated with recombination rate in all three species,
420 except gene flow in *L. vociferans* (Figure S16; Table S18). Variation in divergence time was not
421 associated with recombination rate in any of the species (Table S18).
422 To further explore the signal for gene flow across the genome, we estimated D and fdm
423 statistics using window-based ABBA-BABA tests in 100kb non-overlapping sliding windows.
424 We found little evidence for gene flow between populations of all three species, except between
425 Belem and Xingu populations of *P. nigromaculata.* The gene flow inferred between these two
426 populations of *P. nigromaculata* was associated with recombination rate (Figure 2, S1, S4). For

427 *L. vociferans* despite the lack of genetic structure, the D statistics failed to find any significant
428 levels of introgression, likely due to the high levels of gene flow among all three populations,
429 violating the ABBA-BABA model.
430
431 **Discussion**
432 Biogeographic patterns of Amazonian taxa exhibit a wide array of temporal and spatial
433 divergences in a dynamic landscape (Smith et al. 2014; Lynch Alfaro et al. 2015; Penz et al.
434 2015; de Oliveira et al. 2016; Byrne et al. 2018; Dagosta and De Pinna 2019; Silva et al. 2019).
435 We found that genomic architecture adds an underappreciated layer of complexity that can
436 obscure inferring the origins of the extraordinary Amazonian diversity by directly impacting the
437 estimation of patterns of differentiation. Our study indicates that the interplay of selection, gene
438 flow, and recombination shaped the genomic landscape of genetic diversity and in turn produced
439 varying levels of phylogenetic signals across the genome. By exploring the effects of genomic
440 architecture on phylogenetic and demographic parameter estimation across species with differing
441 degrees of gene flow, we showed that accounting for the processes that produce an
442 heterogeneous genomic landscape helps clarify interpretations on the geographic differentiation
443 of Amazonian taxa.
444
445 *Applying genomic-architecture aware approaches to Amazonian biogeography*
446 We found that introgression, even if ancestral, can produce a highly heterogeneous
447 landscape of phylogenetic conflict compromising biogeographic inference across Amazonia. For
448 example, in *P. nigromaculata*, gene flow between non-sister taxa, as estimated with our model-
449 based approach, was positively associated with support for an alternative topology (topology 2)

and recombination rate. This pattern likely affected genome-wide species tree and topology weight analyses. In contrast, the topology reflecting the most probable species tree (topology 1) was considerably more frequent in windows with low recombination rates. The phylogenetic conflict between alternative topologies has practical biogeographical implications. Support for topology 2 for *P. nigromaculata* would indicate the taxa diverged via a stepping-stone process from the west through the Tapajos, Xingu, and Belem regions, consistent with the Moisture Gradient Hypothesis (Silva et al. 2019). In contrast, if topology 1 reflects the population history of *P. nigromaculata*, it would indicate an opposite scenario, with an ancestral population in southeastern Amazonia, which could be linked to physiographic changes in the landscape (Albert et al. 2018; Musher et al. 2021). The results we obtained here are in agreement with simulations and empirical studies suggesting that in the presence of gene flow, low recombination areas are more prone to maintain the ancient branching signal (Li et al. 2019; Tigano et al. 2021). The strong linkage in low recombination regions should lead to the more effective removal of alleles introduced by hybridization that are more likely to be deleterious (Nachman and Payseur 2012; Schumer et al. 2018). Although the phylogenetic signal were more stable across the genomes of *X. spixii* and *L. vociferans*, it was also predicted by recombination rate and gene flow. Interestingly, in *L. vociferans*, we found substantially higher weights for the putative species-tree topology in regions of low recombination despite the lack of genetic structure across rivers (Figure 5), suggesting that spatial diffusion of alleles in a continuous population was also driven by genomic architecture. Collectively, these results indicate that genome-wide estimates of biogeographically relevant parameters might not recapitulate the effects of historical landscape changes on the genome.

We did not find any association between divergence time and recombination rate in our

model-based approach. This finding suggests that, by modeling gene flow and intra-locus recombination, we were able to obtain relatively stable estimates for divergence time across the genome. Simulation studies have reported that clades with a history of introgression will show extensive branch length distortion in bifurcating phylogenetic methods, depending on the age, direction, and intensity of gene flow (Leaché et al. 2014). We found that not accounting for gene flow and genomic architecture will likely impact divergence times estimates in phylogenetic approaches. Gene flow was considerably skewed towards lower values by selection and varied accordingly with the recombination rate. In this sense, even methods designed to incorporate gene flow into phylogenetic estimations such as phylogenetic network approaches (Solís-Lemus and Ané 2016; Wen et al. 2018), might lead to misleading results when considering genome-wide markers. Although phylogenetic networks are an ideal way to track the presence of gene flow, it might be difficult to disentangle the processes driving phylogenetic conflict, given that estimated introgression proportions might be biased by the genomic landscape. The pattern reported here might be common across the thousands of lineages isolated by Amazonian tributaries, given that multiple recent studies have been suggesting extensive introgression across rivers (Weir et al. 2015; Barrera-Guzmán et al. 2018; Ferreira et al. 2018; Berv et al. 2021; Del-Rio et al. 2021; Musher et al. 2021). By exploring the landscape of genomic differentiation in a comparative framework, we were able to directly elucidate the impact of varying gene flow regimes on inferring evolutionary relationships across Amazonia.

Our genome-wide estimates of *Ne* and gene flow were more similar to estimates from regions with signatures of selection versus regions deemed to be evolving neutrally. For instance, areas of the genome estimated to be evolving neutrally had up to 13% larger *Ne* in *P. nigromaculata* and 64% higher gene flow in *X. spixii* than estimates based on genome-wide loci

(Figure 7). These results are in agreement with studies indicating that demographic parameter estimation can be severely affected by positive and background selection (Schrider et al. 2016; Johri et al. 2021; Johri et al.). Natural selection can skew levels of genetic variation in a similar way to certain non-equilibrium demographic histories, often leading to overestimates of population bottlenecks and the rate of demographic expansions (Ewing and Jensen 2016; Schrider et al. 2016). For example, positive selection leading to fixation of large haplotypes linked to the target of selection may mimic population bottlenecks (Wayne and Simonsen 1998), and the recovery from these sweeps, might inflate the proportion of rare variants, resembling recent population expansions (Schrider et al. 2016). Although we did not model demographic changes, summary statistics that are indicative of demographic oscillations such as Tajima's D, varied considerably across the genome, with more negative values in regions of low recombination (Figure 2). Predictions for the historical demography of populations are explicitly linked to commonly tested Amazonian diversification hypotheses [e.g., the refugia hypothesis (Haffer 1969)], and understanding how drift and selection have shaped different regions of the genome will be key to building more nuanced biogeographic models. Our examination of three codistributed species showed that the effect of selection on demographic analyses was a general phenomenon that can have a profound effect on modeling biogeographic dynamics.

Our data show pervasive signatures of selection across the genome of three co-occurring species. We estimated that on average 31.6% (accounting for false positives) of the genome of focal species had a high probability (>0.70) for models with selective sweeps or linked selection. Recent estimations for birds and mammals show substantial variation in the proportion of the genome subject to selection, with estimates ranging above 50% (McVicker et al. 2009; Pouyet et al. 2018; Brand et al. 2021; Manthey et al. 2021). Although our data indicate that regions

519 potentially affected by linked selection had a better fit to a bifurcating phylogenetic model, these
520 regions were not suitable for population-level analyses (Schrider et al. 2016; Pouyet et al. 2018).
521 Hence, reconciling phylogenetic inference and demographic parameter estimations in
522 phylogenomic approaches might demand recombination and selection-aware approaches
523 (Charlesworth and Jensen 2021). By characterizing the genomic landscape, the effect of selection
524 in demographic parameter estimations can be mitigated by targeting genomic regions as distant
525 as possible from potential targets of selection such as genes and functional elements, as well as
526 avoiding areas of low recombination or affected by biased gene conversion (Pouyet et al. 2018).
527 A key problem with selecting loci with distinct characteristics is that current methods designed to
528 estimate recombination and selection across the genome achieve optimal performance when the
529 demographic history of a population is known (Dapper and Payseur 2018; Harris et al. 2018;
530 Rousselle et al. 2018; Johri et al. 2020). On the other hand, demographic parameters may be
531 heavily biased when recombination and selection are neglected (Ewing and Jensen 2016; Pouyet
532 et al. 2018). This conundrum indicates that methods designed to simultaneously account for
533 multiple genomic processes, such as recombination, selection, drift, and mutation (Johri et al.
534 2020; Barroso and Dutheil 2021; Johri et al. 2021), associated with simulation studies (Tigano et
535 al. 2021) might be necessary to unbiasedly estimate evolutionary parameters from genome-wide
536 variation.
537
538 *Heterogeneous genomic landscapes within and between species*
539 The genomic landscapes of our focal species were highly heterogeneous and presented
540 some key differences between species. Chromosome size was a good predictor of genetic
541 diversity, recombination rate, and phylogenetic signal in two of the species (*P. nigromaculata*

and *X. spixii*). The lack of association between chromosome size and genomic characteristics in *L. vociferans* was unexpected given that, during meiosis, chromosome segregation often requires at least one recombination event per homologous chromosome pair (Fledel-Alon et al. 2009), leading to higher recombination rates in shorter chromosomes (Kaback et al. 1992; Farré et al. 2012; Kawakami et al. 2014; Haenel et al. 2018; Manthey et al. 2021). This lack of association has also been observed in other species of birds and mammals (Pessia et al. 2012; Dutoit, Burri, et al. 2017; Kartje et al. 2020) and could be explained by a reduced synteny between our references and the zebra finch genome, or the historical demography of the species, which in some cases can reverse the expected associations between recombination, genetic diversity, and chromosome size (Van Belleghem et al. 2018; Tigano et al. 2021). However, the former scenario was less likely due to the relative stability of chromosomes across avian species (Ellegren 2010).

The concordant patterns of genetic diversity and differentiation across the genomes of isolated populations within species indicated that genomic architecture was likely conserved over the population history of our focal taxa, as observed in other systems (Dutoit, Vijay, et al. 2017; Van Doren et al. 2017; Vijay et al. 2017; Delmore et al. 2018; Tigano et al. 2021). For example, consistent variation in *Fst* values across the genome of population pairs of the same species was likely reflecting the genomic landscape of the ancestral population. Regions of low recombination and *Ne* in the parent population would promote faster differentiation between daughter populations after isolation. These results agree with the idea that in birds, recombination hotspots are associated with gene promoters, which might help maintain a conserved landscape of recombination across lineages that span for millions of years (Singhal et al. 2015).

Identifying the driving forces shaping patterns of diversity along the genome of non-

model organisms is a major endeavor in modern genomics and is critical to understand how theoretical models and patterns observed in model organisms extend to natural systems (Comeron 2014; Elyashiv et al. 2016; Stankowski et al. 2019; Barroso and Dutheil 2021). In this study, we demonstrate that the interplay between recombination and selection had a strong impact on phylogenetic inference and demographic parameter estimates. However, other genomic processes might be contributing to this pattern. For instance, levels of polymorphism across the genome could be derived from variation in mutation rate (Jónsson et al. 2018; Smith et al. 2018; Besenbacher et al. 2019; Barroso and Dutheil 2021). Non-crossover gene conversion (Korunes and Noor 2017), where DNA strands break during meiosis and are repaired based on homologous sequences without crossing-over, and crossover events could be mutagenic, leading to higher mutation rates in areas of higher recombination (Arbeithuber et al. 2015; Korunes and Noor 2017). Simulation studies have rejected gene conversion as a process driving genome-wide patterns of genomic diversity in relatively recent divergence events (Tigano et al. 2021) and empirical studies suggest that mutations associated with crossover events occur at relatively low frequencies (Halldorsson et al. 2019). Although differential mutation rate across the genome might not explain the strong association between genetic diversity and genomic architecture, the majority of the variation in genetic diversity in our focal species was not explained by recombination. This suggests that variation in mutation rate, not associated with recombination, could be playing a role in the genomic landscape of genetic diversity. It is important to note that irrespective of the processes driving the heterogeneous levels of genetic variation across the genome, these biases on genome-wide phylogenetic and population genetics inferences may remain unless the multitude of parameters varying across the genome are modeled in a unifying approach (Johri et al. 2021). Until then, genomic-architecture-aware approaches might be

588 essential to disentangle the effects of intrinsic genomic characteristics and selection from neutral
589 processes.
590
591 **Conclusions**
592 We present comparative empirical evidence of systematic biases in estimating genome-wide
593 evolutionary parameters in one of the most well-studied biogeographic models on earth. The
594 interplay between recombination, selection, and gene flow produced a highly heterogeneous
595 landscape of genetic diversity and differentiation within and between species, where typically
596 used methods might fail to recapitulate the effects of landscape evolution on the genome.
597 Phylogenetic approaches and demographic parameter estimation are essential to test alternative
598 hypotheses of diversification (Knowles 2009) and have been extensively used in
599 phylogeographic studies across Amazonia (Aleixo 2004; Fernandes et al. 2012; Ribas et al.
600 2012; Capurucho et al. 2013; Fernandes et al. 2013; Thom and Aleixo 2015). Allopatric
601 differentiation and secondary contact are potentially the most common modes of speciation in
602 Amazonia producing widespread differentiation across the genome due to the effects of genetic
603 drift and within-population selection. These processes lead to a background pattern of
604 differentiation that was likely to be associated with genomic architecture (Manthey et al. 2021),
605 however, patterns of association might not be concordant between species. Comparative studies
606 in biogeography often report idiosyncratic patterns across multiple levels of populations
607 histories, with heterogeneous patterns of differentiation and contrasting divergence times
608 associated with the same geographic barrier (Smith et al. 2014; Naka and Brumfield 2018; Silva
609 et al. 2019; Provost et al. 2021), and idiosyncratic population size changes over time (Bai et al.
610 2018; Thom et al. 2020; Carvalho et al. 2021). Our results suggest that genomic architecture

should be considered as another level of complexity that is also subject to idiosyncrasies between species.

Material and methods

Studied species, sampling design and whole-genome sequencing

We selected three species with populations occurring in southeastern Amazonia occurring in distinct forest strata of upland forest habitats: 1) *Phlegopsis nigromaculata,* an obligatory army-ant follower restricted to the understory, with three distinct subspecies isolated by Xingu and Tocantins rivers with considerable levels of genetic differentiation (A. Aleixo et al. 2009); 2) *Xiphorhynchus spixii,* which occupies the midstory of eastern Amazonian forests, and has two structured populations divided by the Xingu River (Aleixo 2004); 3) *Lipaugus vociferans,* a widespread canopy species, without genetic structure reported across rivers.

To optimize the spatial representation of our samples, we selected a single individual per locality targeting approximately 10 individuals per interfluve per species (Tapajos, Xingu, and Belem), yielding a total of 31, 31, and 26 samples for *P. nigromaculata, L. vociferans*, and *X. spixii*, respectively (Table S1; Figure 1). We isolated genomic DNA from muscle tissue preserved in alcohol (65 samples) and skin from the toe pads of museum specimens (31 samples). All samples were loaned from the Museu Paraense Emilio Goeldi (MPEG). From tissues, we extracted DNA with Qiagen high molecular weight DNA kit (MagAttract HMW DNA Kit - Qiagen). For the toe pads, we performed a protocol specific for degraded DNA consisting of additional steps for washing the samples with H_2O and EtOH prior to extracting and extra time for digestion. We modified the DNeasy extraction protocol (DNeasy Blood & Tissue Kits - Qiagen) by replacing the standard spin columns with the QIAquick PCR filter

columns (QIAquick PCR Purification Kit - Qiagen), selecting for smaller fragments of DNA, typically found in degraded samples. Toe pad extractions were conducted on a dedicated lab for working with historical samples at the American Museum of Natural History (AMNH) to reduce contamination risk. We quantified DNA extracts using a Qubit 2.0 Fluorometer (Thermo Fisher Scientific). Illumina libraries with variable insert sizes were generated and samples were sequenced by Rapid genomics (Gainesville, Florida) to ~10x coverage using 3.5 lanes of paired-end (2x150 bp) Illumina S4 NovaSeq 6000. Raw reads were initially trimmed and filtered using trimmomatic v0.36 (Bolger et al. 2014).

Genomic reference, gene annotation and outgroups

We obtained reference genomes from closely related species. For *P. nigromaculata,* we used as reference the genome of *Rhegmatorhina melanosticta* (Coelho et al. 2019) with TMRCA = 9.60Ma (Harvey et al. 2020). For *X. spixii,* we used the genome of *X. elegans* (GCA_013401175.1 ASM1340117v1; NCBI genome ID: 92877; Feng et al. 2020) with TMRCA = 2.36Ma (Harvey et al. 2020), and for *L. vociferans* we used the genome of *Cephalopterus ornatus* (GCA_013396775.1 ASM1339677v1; NCBI genome ID: 92752; Feng et al. 2020) with TMRCA =15.10Ma (Harvey et al. 2020). Given that bird chromosomes are known to have high synteny and evolutionary stasis between distantly related species (Ellegren 2010), we produced a pseudo-chromosome reference genome for *X. elegans* and *C. ornatus* by ordering and orienting their scaffolds to the 35 chromosomes of the Zebra Finch (*Taeniopygia guttata*; version taeGut3.2.4) with chromosemble in satsuma v3.1.0 (Grabherr et al. 2010). For *R. melanosticta,* we used the chromosome assignment conducted in a previous study (Coelho et al. 2019). To check the completeness of our pseudo-chromosome references, we used Busco v2.0.1

(Waterhouse et al. 2018) to search for a set of single-copy avian ortholog loci. To transfer genome annotations from the scaffold assemblies to the pseudo chromosome reference genomes, we mapped the genomic coordinates of each annotated feature using gmap (Wu and Watanabe 2005). For *R. melanosticta* we used the annotation performed by Mikkelsen and Weir (2020) and for X. *elegans* and *L. vociferans*, we used the annotations performed by Feng et al. (2020). A total of 98.90% (15,195), 97.46% (14,834 genes), and 98.92% (15,599 genes) of all annotated genes in *R. melanosticta*, *X. elegans*, and *C. ornatus* were successfully mapped to the pseudo-chromosome reference, respectively.

We downloaded raw reads from additional closely related species that were used as outgroups in phylogenetic analyses. For *P. nigromaculata*, we included *R. melanosticta*, *Sakesphorus luctuosus* (GCA_013396695.1 ASM1339669v1; NCBI genome ID: 92896; Feng et al. 2020) and *X. elegans* as outgroups. For *X. spixii*, we included *X. elegans*, *S. luctuosus*, *Campylorhamphus procurvoides* (GCA_013396655.1 ASM1339665v1; NCBI genome ID: 92894; Feng et al. 2020), and *Furnarius figulus* (GCA_013397465.1 ASM1339746v1; NCBI genome ID: 92763; Feng et al. 2020). For *L. vociferans*, we included *C. ornatus*, *Pachyramphus minor* (GCA_013397135.1 ASM1339713v1; NCBI genome ID: 92755; Feng et al. 2020), and *Tyrannus savana* (GCA_013399735.1 ASM1339973v1; NCBI genome ID: 92814; Feng et al. 2020).

Read alignment, variant calling and filtering

Trimmed and filtered reads were aligned to the references in BWA v0.7.17 (Li and Durbin 2009) using default parameters. We used Picard v.2.0.1 (Broad Institute, Cambridge, MA; http://broadinstitute.github.io/picard/) to 1) sort sam files with SortSam; 2) reassign reads to

groups with AddOrReplaceReadGroups; 3) identify duplicated reads with Markduplicates; 4) calculate summary statistics with CollectAlignmentSummaryMetrics, CollectInsertSizeMetrics, and CollectRawWgsMetrics; and 5) create indexes with BuildBamIndex. All Picard functions were run with default parameters. We used the standard GATK v3.8 (McKenna et al. 2010) pipeline to 1) call SNPs and Indels for each individual separately with HaplotypeCaller; 2) perform genotyping with GenotypeGVCFs, assuming a value of 0.05 for the --heterozygosity flag; 3) flag and filter variants with VariantFiltration. Given the lack of a high confidence SNP panel, we implemented hard filtering options recommended by the Broad Institute's Best Practices (https://gatk.broadinstitute.org/). We filtered SNPs with quality by depth below 2 (QD < 2.0), SNPs where reads containing the alternative allele were considerably shorter than reads with the reference allele (ReadPosRankSum < -8), SNPs with root mean square of the mapping quality lower than 40 (MQ < 40.0), SNPs with evidence of strand bias (FS > 60.0 and SOR > 3.0), and SNPs where the read with the alternative allele had a lower mapping quality than the reference allele (MQRankSumTest < − 12.5). Lastly, we filtered raw VCF files by keeping only bi-allelic sites, with no more than 50% of missing information, with a minimum read depth of 4 and maximum of 30, and read quality score > Q20 using VCFTOOLS v0.1.15 (Danecek et al. 2011). We phased the genotypes in our genomic vcf files using BEAGLE v5.1 (Browning and Browning 2007; Browning et al.) in sliding windows of 10kb and overlap between windows of 1kb.

Recombination, window-based summary statistics, and genetic structure

To estimate recombination rate (r = recombination rate per base pair per generation) from population level data for each of the species complexes we used ReLERNN (Adrion et al. 2020).

This approach estimates the genomic landscape of recombination by leveraging recurrent neural networks using the raw genotype matrix as a feature vector, avoiding the need to convert the data into summary statistics. ReLERNN calculates r by simulating data matching the θW of the observed DNA sequences. Simulations are then used to train and test a recurrent neural network model designed to predict the per base recombination rate across sliding windows of the genome. Given that genetic structure could potentially influence ReLERNN estimates (Mezmouk et al. 2011; Mangin et al. 2012), we restricted our analyses to the individuals of the Tapajos interfluve, that was composed exclusively of recent tissue samples, and we did not find any sign of population substructure in the three lineages (see below). Although we did not estimate r for all populations, the landscape of recombination across bird lineages is considered conserved, and variation between recently diverged populations should be minimal (Singhal et al. 2015). To account for the historical demography of the populations, we provided to ReLERNN the output of our SMC++ analyses (see below) with the --demographicHistory option. We considered a mutation rate of 2.42×10^{-9} mutations per generation and one year generation time (Jarvis et al. 2014; Zhang et al. 2014).

We calculated population genomics summary statistics for sliding windows using scripts available at https://github.com/simonhmartin/genomics_general. We initially converted vcf files per species into geno format, using parseVCF.py. *Fst*, *Dxy*, and π were calculated for the different populations in each of three interfluves using popgenWindows.py. We estimated the D statistics in sliding windows using the ABBABABAwindows.py. We used species tree topology with the highest probability from our species tree analyses (see *Phylogenomic analyses, and topology weighting*)treating the Tapajos, Xingu and Belem populations as the terminals. For all summary statistics, we used phased vcf files, setting the window size to 10kb (-w option) without

overlap between windows and the minimum number of sites without missing information per window to 500 (-m option). To obtain GC content estimates across 100kb windows for our reference genomes, we used sequir v4.2 (Charif and Lobry 2007) in R. We fit general linear regressions and Pearson's correlation index between population genetics summary statistics, phylogenetic weights, and genomic architecture estimates in R. To account for the potential non-linearity of these relationships, we also fit a LOESS model using the R package caret (Kuhn 2008). Models were trained using leave-one-out cross-validation of 80% of the total data.

To explore the genome-wide pattern of genetic structure, we performed Principal Component Analysis (PCA) and individuals relatedness analyses based on identity-by-descent using SNPRelate v1.20.1 (Zheng et al. 2012) in R. In order to minimize the effect of missing genotypes in the PCA, we filtered our vcf files to keep SNPs present in at least 70% of the individuals. We also used SNPRelate to perform an identity-by-state (IBS) analysis among individuals for each species. To avoid the influence of SNP clusters in our PCA and IBS analysis, we pruned SNPs in approximate linkage equilibrium (LD>0.2) with each other.

Specific regions of the genome might be differently affected by selection and gene flow, exhibiting different levels of genetic diversity and differentiation between populations (Ellegren et al. 2012; Langley et al. 2012; Li et al. 2019). To explore the genomic variation in genetic structure we used lostruct (Li and Ralph 2019). This approach 1) summarizes the relatedness between individuals across genomic windows using PCA, 2) calculates the pairwise dissimilarity in relatedness among window, 3) uses multidimensional scaling (MDS) to produce a visualization of how variable patterns of relatedness are across the genome, and 4) allows the user to combine regions by similarity to inspect contrasting patterns of genetic structure across the genome. We ran lostruct for windows with 1000 SNPs, allowing for 30% of missing

749 genotypes. To visualize the results, we selected the 10% of the windows closer to the three
750 further points on the two first MDS coordinates and performed individual PCA analysis on
751 clustered windows.
752
753 *Historical demography, selective sweeps, and linked selection*
754 We estimated variations on effective population sizes through time using unphased
755 genomes in SMC++ v1.15.3 (Terhorst et al. 2017). Our goal with this approach was to estimate
756 past fluctuations in *Ne* to be included in ReLERNN (Adrion et al. 2020) and DiploS/HIC (Kern
757 and Schrider 2018) models to account for historical demography. We ran SMC++ exclusively for
758 the Tapajos population of each species assuming a mutation rate of 2.42×10^{-9} mutations per
759 generation and one year generation time (Jarvis et al. 2014; Zhang et al. 2014). We explored
760 historical demography of populations within a time window between the present and 300,000ya.
761 To detect signatures of selection across the genome we used a Supervised Machine
762 Learning (SML) approach implemented in diploS/HIC (Kern and Schrider 2018). This approach
763 used coalescent simulations of genomic windows to train and test a Convolutional Neural
764 Network (CNN) designed to predict hard and soft selective sweeps and genetic variation linked
765 to selective sweeps across sliding windows of the genome. Genomic windows were simulated
766 using discoal (Kern and Schrider 2016) according to five distinct models: 1) hard selective
767 sweep; 2) soft selective sweep; 3) neutral variation linked to soft selective sweep; 4) neutral
768 variation linked to hard selective sweep; and 5) neutral genetic variation. We performed 5,000
769 simulations per model using 220kb genomic windows divided into 11 subwindows. To account
770 for the neutral demography of the populations, which is essential to obtain robust model
771 classification between windows (Harris et al. 2018), we added demographic parameters

772 estimated with SMC++ into discoal simulations. To account for uncertainty in simulated
773 parameters, we followed the approach of Manthey et al. (2021) by allowing current *Ne* to vary
774 between ⅓ to 3x the estimated value obtained with SMC++ within a uniform distribution.
775 Population scaled recombination rate (rho=4Ner; where r is the recombination rate estimated
776 with ReLERNN) priors were set based on the minimum and maximum values obtained across
777 windows with ReLERNN. We set a uniform prior for selection coefficients ranging from
778 0.00025 to 0.025, and we conditioned sweep completion between the present and 10,000
779 generations ago. We used a uniform prior between 0.01 and 0.2 for the initial frequency of
780 adaptive variants in soft sweep models. Simulations were converted into feature vectors
781 consisting of population genetics summary statistics, taking into account the observed amount of
782 missing data by using a genomic mask. We estimated the probability of alternative models for
783 observed windows of 20kb. We ran CNNs for 1000 epochs, stopping the run if validation
784 accuracy did not improve for 50 consecutive epochs. We ran five independent runs and predicted
785 observed data with the run that provided the highest accuracy on testing data. To assess the
786 classification power of the CNNs, we inspected the overall accuracy, the false positive rate
787 (FPR), recall (the number of correct positive predictions made out of all positive predictions that
788 could have been made), and area under the curve (AUC). To acknowledge the uncertainty in
789 model selection, we only assigned a model with a probability higher than 0.7 to a genomic
790 window.
791
792 *Phylogenomic analyses, and topology weighting*
793 To estimate phylogenetic relationship between individuals, we estimated supermatrix
794 trees concatenating all SNPs using IQTree2 (Minh et al. 2020). We converted vcf files to phylip

format using vcf2phylip.py (Ortiz 2019), randomly resolving heterozygous genotypes, and keeping SNPs present in at least 80% of the individuals. In IQTree2 we ran a total of 1000 bootstrap replicates and controlled for ascertainment bias assuming a GTR+ASC substitution model. To estimate phylogenetic trees based on sliding windows of phased vcf files, we used PHYML v3.0 (Guindon et al. 2010) following (Martin and Van Belleghem 2017). We tested windows with different amounts of information content, selecting regions with 50, 100, 500 and 1000 SNPs. We conducted 100 bootstrap replicates per window. To estimate unrooted topology weight for each window across the genome, we used Twisst (Martin and Van Belleghem 2017). This approach allowed us to quantify the relationships among taxa that are not necessarily monophyletic, providing an assessment of the most likely topology for a given genomic region. Given that windows with different information content yielded similar results for the topology weights across the genome, we only present the results for 100 SNPs windows (average window size of 14,503 bp, 15,637 bp, and 5,821 bp for *P. nigromaculata, X. spixii*, and *L. vociferans*, respectively) in subsequent analyses.

To estimate the posterior probability of unrooted species trees, we used Astral-III v5.1.1 (Zhang et al. 2018; Rabiee et al. 2019), using the gene trees produced with phyml as inputs. We used Astral to score unrooted trees (-q option), estimating their quartet score, branch lengths, and branch support. We set as our main topology (outgroup,Belem(Xingu,Tapajos), and used the -t 2 option to calculate the same metrics for the first alternative and second alternative topologies. Given we only have four terminals per lineage (3 populations + outgroup), three are only three possible unrooted trees. Therefore, this approach allowed us to calculate the posterior probability of all possible topologies. We conducted this approach for the whole set of gene trees and also for subsets of the data, based on specific characteristics of each window. To assess how support

for a specific topology varies based on thresholds for specific summary statistics, we selected windows across the genome with the upper and lower 10% tile for recombination rate, Fst, π, *Dxy* and D statistics.

Model based approach to account for recombination and selection.

In order to explicitly account for gene flow while testing for alternative topologies and estimating demographic parameters of genomic windows, we used a combination of coalescent simulations and supervised machine learning. We simulated data under three alternative topologies, matching the unrooted trees tested in our phylogenetic approach: topology 1) (out, (Belem,(Xingu,Tapajos))); topology 2) (out,(Tapajos,(Xingu,Belem))); topology 3) (out,(Xingu, (Tapajos,Belem))). We allowed for constant gene flow after the divergence between Xingu and Belem, and Xingu and Tapajos populations. We did not allow gene flow between Belem and Tapajos due to the geographic disjunction between these populations. We simulated 5,000 loci of 10kb, using uniform and wide priors for all parameters (Table S19), and performed 1 million simulations per model. We assumed a fixed mutation rate of 2.42×10^{-9} mutations per generation and one year generation time (Jarvis et al. 2014; Zhang et al. 2014). Genetic data for each model was simulated in PipeMaster (Gehara et al. 2017) which allows for a user-friendly implementation of msABC (Pavlidis et al. 2010). We summarized genetic variation of observed and simulated data in a feature vector composed of population genetics summary statistics, including mean and variance across loci: number of segregating sites per population and summed across populations, nucleotide diversity per population and for all populations combined, Watterson's theta (Watterson 1975) per population and for all populations combined, pairwise *Fst* between populations, number of shared alleles between pairs of populations, number of

private alleles per population and between pairs of populations, and number of fixed alleles per population and between pairs of populations. To align loci across individuals, phased vcf files per population were split every 10kb windows and converted into a fasta format including monomorphic sites using bcftools (Li 2011). Fasta alignments were converted into feature vectors with PipeMaster which uses PopGenome (Pfeifer et al. 2014) in R. To obtain a genome-wide estimate of demographic parameters, we selected one 10kb genomic window every 100kb to reduce the effect of linkage between windows, and we subsampled 5,000 windows from this data set. We explored how simulated models fitted the observed data PCAs by plotting the first four PCs of simulated statistics vs observed. We also generated goodness-of-fit plots using the gfit function of abc v2.1 (Csilléry et al. 2012) in R.

To classify observed datasets into our three models, we used a Neural Network (nnet) implemented in Keras v2.3 (https://github.com/rstudio/keras) in R. After an initial exploration for the best architecture for our nnet, we conducted our final analyses using three hidden layers with 32 internal nodes and a “relu” activation function. The output layer was composed of three nodes and a “softmax” activation function. 25% of the simulations were used as testing data. We ran the training step for 1000 epochs using “adam” optimizer and a batch size of 20,000. 5% of the training data set was used for validation, and we used accuray and a sparse_categorical_crossentropy for the loss function to track improvements in model classification. For the most probable model considering genome-wide windows per species, we estimated demographic parameters with a nnet with a similar architecture but designed to predict continuous variables. For this step, we used an output layer with a single node and a “relu” activation. In the training step, we used the mean absolute percentage error (MAE) as an optimizer, training the nnet for 3000 epochs with batch size of 10,000 and a validation split of

0.1. We ran this procedure 10 times for each demographic parameter and summarized the results by calculating the mean across estimates. To additionally assess the accuracy of parameter estimation we calculated the coefficient of correlation between estimated and true simulated values of the testing data set. To explore how genome-wide parameter estimation differs from regions with distinct signature of selection and under neutrality, we created subsets of 10kb windows that were assigned with high probability (> 0.70) to one of the five distinct models implemented in diploS/HIC. For each species, we estimated parameters based on the best model (topology) considering genome-wide windows. We selected up to 1000 windows for each of the five selection classes and performed the same approach as described above.

To obtain window-based model probability and demographic parameter estimates, we used a similar approach as described above but simulating 100kb window size and using a modified version of PipeMaster (Gehara et al. 2017) that allowed us to simulate intra locus recombination. By selecting a larger window size we increased the information content and resolution of summary statistics of single genomic windows. We performed 100,000 simulations per model, and used the same uniform priors for all parameters as implemented above. For intralocus recombination, we set a uniform prior ranging from 0 to the higher estimated value with ReLERNN per species (*P. nigromaculata* = 3.021×10^{-9}; *X. spixii* = 2.475×10^{-9}; *L. vociferans* = 2.171×10^{-9}).

Lastly, to explore how recombination rate and gene flow impact topology weight, we performed coalescent simulations based on demographic parameters estimated for *P. nigromaculata*, and calculated topology weights using Twisst (Martin and Van Belleghem 2017). We simulated 1,000 windows of 10kb for four models varying the presence of intra-locus recombination and gene flow between Xingu and Belem, assuming topology 1 (three ingroups

887 plus one outgroup). Simulated parameters are available on Table S20. Simulations were
888 performed with PipeMaster, and we converted the ms output to phylip format with PopGenome.
889 We ran trees for each 10 kb window with IQTREE-2 using default parameters and ran Twisst on
890 this estimated set of trees (Figure S15).
891
892 **Acknowledgments**
893 We would like to thank K. Provost, J. Merwin, V. Chua, E. Tenorio, J. Cracraft, P. Sweet, T.
894 Trombone, B. Bird, L. Musher. We also thank the Museu Paraense Emílio Goeldi—MPEG for
895 tissue samples. All genetic samples were included on the SisGen platform under the protocols
896 AA7DDBF and AB8BB93. G.T. was funded by the Frank M. Chapman memorial fund of the
897 American Museum of Natural History. Romina Batista received support from Coordenação de
898 Aperfeiçoamento de Pessoal de Nível Superior – Brasil (CAPES-INPA proc.
899 88887477562/2020-00). B.T.S. was supported by awards from the National Science Foundation
900 US (DEB-1655736; DBI-2029955).
901
902 **Data availability**
903 The raw genetic data underlying this article are available in NCBI short read archive at
904 Bioproject # (accession numbers will be provided upon acceptance). All code and source datasets
905 needed to replicate this study are available at https://doi.org/number will be provided upon
906 acceptance (zenodo):https://github.com/GregoryThom/Genomic-architecture-Amazonian-birds.
907
908 **References**

909 Adrion JR, Galloway JG, Kern AD. 2020. Predicting the Landscape of Recombination Using
910 Deep Learning. *Mol. Biol. Evol.* 37:1790–1808.

911 Albert JS, Craig JM, Tagliacollo VA, Petry P. 2018. Upland and lowland fishes: a test of the
912 river capture hypothesis. *Mountains, climate and biodiversity*:273–294.

913 Aleixo A. 2004. Historical diversification of a terra-firme forest bird superspecies: a
914 phylogeographic perspective on the role of different hypotheses of Amazonian
915 diversification. *Evolution* 58:1303–1317.

916 Aleixo A, Burlamaqui TCT, Schneider MPC. 2009. Molecular Systematics and Plumage
917 Evolution in the Monotypic Obligate Army-Ant-Following Genus Skutchia
918 (Thamnophilidae). *Condor* 111:382-387.

919 Arbeithuber B, Betancourt AJ, Ebner T, Tiemann-Boege I. 2015. Crossovers are associated with
920 mutation and biased gene conversion at recombination hotspots. *Proc. Natl. Acad. Sci. U. S.*
921 *A.* 112:2109–2114.

922 Barrera-Guzmán AO, Aleixo A, Shawkey MD, Weir JT. 2018. Hybrid speciation leads to novel
923 male secondary sexual ornamentation of an Amazonian bird. *Proceedings of the National*
924 *Academy of Sciences* 115:E218–E225.

925 Barroso GV, Dutheil JY. 2021. Unpublished data,
926 https://www.biorxiv.org/content/10.1101/2021.09.16.460667.abstract, last accessed
927 November 25, 2021.

928 Bates JM, Hackett SJ, Cracraft J. 1998. Area-relationships in the Neotropical lowlands: an
929 hypothesis based on raw distributions of Passerine birds. *Journal of Biogeography* 25:783–
930 793.

931 Berv JS, Campagna L, Feo TJ, Castro-Astor I, Ribas CC, Prum RO, Lovette IJ. 2021. Genomic
932 phylogeography of the White-crowned Manakin Pseudopipra pipra (Aves: Pipridae)
933 illuminates a continental-scale radiation out of the Andes. *Mol. Phylogenet. Evol.*:107205.

934 Besenbacher S, Hvilsom C, Marques-Bonet T, Mailund T, Schierup MH. 2019. Direct estimation
935 of mutations in great apes reconciles phylogenetic dating. *Nat Ecol Evol* 3:286–292.

936 Bolger AM, Lohse M, Usadel B. 2014. Trimmomatic: a flexible trimmer for Illumina sequence
937 data. *Bioinformatics* 30:2114–2120.

938 Brand CM, White FJ, Ting N, Webster TH. 2021. Unpublished data,
939 https://www.biorxiv.org/content/10.1101/2020.12.14.422788v3.abstract, last accessed
940 November 25, 2021.

941 Brandvain Y, Kenney AM, Flagel L, Coop G, Sweigart AL. 2014. Speciation and introgression
942 between Mimulus nasutus and Mimulus guttatus. *PLoS Genet.* 10:e1004410.

943 Browning BL, Zhou Y, Browning SR. A one penny imputed genome from next generation
944 reference panels. *Am. J. Hum. Genet.* 103(3):338-348

945 Browning SR, Browning BL. 2007. Rapid and accurate haplotype phasing and missing-data

946 inference for whole-genome association studies by use of localized haplotype clustering.
947 *Am. J. Hum. Genet.* 81:1084–1097.

948 Burri R, Nater A, Kawakami T, Mugal CF, Olason PI, Smeds L, Suh A, Dutoit L, Bureš S,
949 Garamszegi LZ, et al. 2015. Linked selection and recombination rate variation drive the
950 evolution of the genomic landscape of differentiation across the speciation continuum of
951 Ficedula flycatchers. *Genome Res.* 25:1656–1665.

952 Byrne H, Lynch Alfaro JW, Sampaio I, Farias I, Schneider H, Hrbek T, Boubli JP. 2018. Titi
953 monkey biogeography: Parallel Pleistocene spread by Plecturocebus and Cheracebus into a
954 post-Pebas Western Amazon. *Zool. Scr.* 47:499–517.

955 Charif D, Lobry JR. 2007. SeqinR 1.0-2: A Contributed Package to the R Project for Statistical
956 Computing Devoted to Biological Sequences Retrieval and Analysis. In: Bastolla U, Porto
957 M, Roman HE, Vendruscolo M, editors. Structural Approaches to Sequence Evolution:
958 Molecules, Networks, Populations. Berlin, Heidelberg: Springer Berlin Heidelberg. p. 207–
959 232.

960 Charlesworth B. 1998. Measures of divergence between populations and the effect of forces that
961 reduce variability. *Molecular Biology and Evolution* 15:538–543

962 Charlesworth B, Jensen JD. 2021. Effects of Selection at Linked Sites on Patterns of Genetic
963 Variability. *Annu. Rev. Ecol. Evol. Syst.* 52:177–197.

964 Charlesworth B, Morgan MT, Charlesworth D. 1993. The effect of deleterious mutations on
965 neutral molecular variation. *Genetics* 134:1289–1303.

966 Chase MA, Ellegren H, Mugal CF. 2021. Positive selection plays a major role in shaping
967 signatures of differentiation across the genomic landscape of two independent Ficedula
968 flycatcher species pairs. *Evolution* 75:2179–2196.

969 Coelho LA, Musher LJ, Cracraft J. 2019. A Multireference-Based Whole Genome Assembly for
970 the Obligate Ant-Following Antbird, Rhegmatorhina melanosticta (Thamnophilidae).
971 *Diversity* 11:144.

972 Comeron JM. 2014. Background selection as baseline for nucleotide variation across the
973 Drosophila genome. *PLoS Genet.* 10:e1004434.

974 Cracraft J. 1985. Historical Biogeography and Patterns of Differentiation within the South
975 American Avifauna: Areas of Endemism. *Ornithol. Monogr.*:49–84.

976 Cruickshank TE, Hahn MW. 2014. Reanalysis suggests that genomic islands of speciation are
977 due to reduced diversity, not reduced gene flow. *Mol. Ecol.* 23:3133–3157.

978 Csilléry K, François O, Blum MGB. 2012. abc: an R package for approximate Bayesian
979 computation (ABC). *Methods Ecol. Evol.* 3:475–479.

980 Cutter AD, Payseur BA. 2013. Genomic signatures of selection at linked sites: unifying the

disparity among species. *Nat. Rev. Genet.* 14:262–274.

Dagosta FCP, De Pinna M. 2019. The Fishes of the Amazon: Distribution and Biogeographical Patterns, with a Comprehensive List of Species. *amnb* 2019:1–163.

Danecek P, Auton A, Abecasis G, Albers CA, Banks E, DePristo MA, Handsaker RE, Lunter G, Marth GT, Sherry ST, et al. 2011. The variant call format and VCFtools. *Bioinformatics* 27:2156–2158.

Dapper AL, Payseur BA. 2018. Effects of Demographic History on the Detection of Recombination Hotspots from Linkage Disequilibrium. *Mol. Biol. Evol.* 35:335–353.

Delmore KE, Lugo Ramos JS, Van Doren BM, Lundberg M, Bensch S, Irwin DE, Liedvogel M. 2018. Comparative analysis examining patterns of genomic differentiation across multiple episodes of population divergence in birds. *Evol Lett* 2:76–87.

Del-Rio G, Rego MA, Whitney BM, Schunck F, Silveira LF, Faircloth BC, Brumfield RT. 2021. Displaced clines in an avian hybrid zone (Thamnophilidae: Rhegmatorhina) within an Amazonian interfluve. *Evolution* https://doi.org/10.1111/evo.14377

Dutoit L, Burri R, Nater A, Mugal CF, Ellegren H. 2017. Genomic distribution and estimation of nucleotide diversity in natural populations: perspectives from the collared flycatcher (Ficedula albicollis) genome. *Mol. Ecol. Resour.* 17:586–597.

Dutoit L, Vijay N, Mugal CF, Bossu CM, Burri R, Wolf J, Ellegren H. 2017. Covariation in levels of nucleotide diversity in homologous regions of the avian genome long after completion of lineage sorting. *Proceedings of the Royal Society B: Biological Sciences* 284:http://dx.doi.org/10.1098/rspb.2016.2756

Edelman NB, Frandsen PB, Miyagi M, Clavijo B, Davey J, Dikow RB, García-Accinelli G, Van Belleghem SM, Patterson N, Neafsey DE, et al. 2019. Genomic architecture and introgression shape a butterfly radiation. *Science* 366:594–599.

Edwards SV, Robin V, Ferrand N, Moritz C. 2021. The evolution of comparative phylogeography: putting the geography (and more) into comparative population genomics. Genome Biol. Evol.: http://dx.doi.org/10.1093/gbe/evab176

Ellegren H. 2010. Evolutionary stasis: the stable chromosomes of birds. *Trends Ecol. Evol.* 25:283–291.

Ellegren H, Smeds L, Burri R, Olason PI, Backström N, Kawakami T, Künstner A, Mäkinen H, Nadachowska-Brzyska K, Qvarnström A, et al. 2012. The genomic landscape of species divergence in Ficedula flycatchers. *Nature* 491:756–760.

Elyashiv E, Sattath S, Hu TT, Strutsovsky A, McVicker G, Andolfatto P, Coop G, Sella G. 2016. A Genomic Map of the Effects of Linked Selection in Drosophila. *PLoS Genet.* 12:e1006130.

1016 Ewing GB, Jensen JD. 2016. The consequences of not accounting for background selection in
1017 demographic inference. *Mol. Ecol.* 25:135–141.

1018 Farré M, Micheletti D, Ruiz-Herrera A. 2012. Recombination Rates and Genomic Shuffling in
1019 Human and Chimpanzee - A New Twist in the Chromosomal Speciation Theory. *Mol. Biol.*
1020 *Evol.* 30:853–864.

1021 Feng S, Stiller J, Deng Y, Armstrong J, Fang Q, Reeve AH, Xie D, Chen G, Guo C, Faircloth
1022 BC, et al. 2020. Dense sampling of bird diversity increases power of comparative genomics.
1023 *Nature* 587:252–257.

1024 Ferreira M, Fernandes AM, Aleixo A, Antonelli A, Olsson U, Bates JM, Cracraft J, Ribas CC.
1025 2018. Evidence for mtDNA capture in the jacamar Galbula leucogastra/chalcothorax
1026 species-complex and insights on the evolution of white-sand ecosystems in the Amazon
1027 basin. *Mol. Phylogenet. Evol.* 129:149–157.

1028 Fledel-Alon A, Wilson DJ, Broman K, Wen X, Ober C, Coop G, Przeworski M. 2009. Broad-
1029 scale recombination patterns underlying proper disjunction in humans. *PLoS Genet.*
1030 5:e1000658.

1031 Fontaine MC, Pease JB, Steele A, Waterhouse RM, Neafsey DE, Sharakhov IV, Jiang X, Hall
1032 AB, Catteruccia F, Kakani E, et al. 2015. Mosquito genomics. Extensive introgression in a
1033 malaria vector species complex revealed by phylogenomics. *Science* 347:1258524.

1034 Garrigan D, Kingan SB, Geneva AJ, Andolfatto P, Clark AG, Thornton KR, Presgraves DC.
1035 2012. Genome sequencing reveals complex speciation in the Drosophila simulans clade.
1036 *Genome Res.* 22:1499–1511.

1037 Gehara M, Garda AA, Werneck FP, Oliveira EF, da Fonseca EM, Camurugi F, Magalhães F de
1038 M, Lanna FM, Sites JW Jr, Marques R, et al. 2017. Estimating synchronous demographic
1039 changes across populations using hABC and its application for a herpetological community
1040 from northeastern Brazil. *Mol. Ecol.* 26:4756–4771.

1041 Gillespie JH. 2000. Genetic drift in an infinite population. The pseudohitchhiking model.
1042 *Genetics* 155:909–919.

1043 Grabherr MG, Russell P, Meyer M, Mauceli E, Alföldi J, Di Palma F, Lindblad-Toh K. 2010.
1044 Genome-wide synteny through highly sensitive sequence alignment: Satsuma.
1045 *Bioinformatics* 26:1145–1151.

1046 Guindon S, Dufayard J-F, Lefort V, Anisimova M, Hordijk W, Gascuel O. 2010. New
1047 algorithms and methods to estimate maximum-likelihood phylogenies: assessing the
1048 performance of PhyML 3.0. *Syst. Biol.* 59:307–321.

1049 Haenel Q, Laurentino TG, Roesti M, Berner D. 2018. Meta-analysis of chromosome-scale
1050 crossover rate variation in eukaryotes and its significance to evolutionary genomics.
1051 *Molecular Ecology* 27:2477–2497.

1052 Haffer J. 1969. Speciation in amazonian forest birds. *Science* 165:131–137.

1053 Haffer J. 2008. Hypotheses to explain the origin of species in Amazonia. *Braz. J. Biol.* 68:917–
1054 947.

1055 Halldorsson BV, Palsson G, Stefansson OA, Jonsson H, Hardarson MT, Eggertsson HP,
1056 Gunnarsson B, Oddsson A, Halldorsson GH, Zink F, et al. 2019. Characterizing mutagenic
1057 effects of recombination through a sequence-level genetic map. *Science*
1058 363:http://dx.doi.org/10.1126/science.aau1043

1059 Harris RB, Sackman A, Jensen JD. 2018. On the unfounded enthusiasm for soft selective sweeps
1060 II: Examining recent evidence from humans, flies, and viruses. *PLoS Genet.* 14:e1007859.

1061 Harvey MG, Bravo GA, Claramunt S, Cuervo AM, Derryberry GE, Battilana J, Seeholzer GF,
1062 McKay JS, O'Meara BC, Faircloth BC, et al. 2020. The evolution of a tropical biodiversity
1063 hotspot. *Science* 370:1343–1348.

1064 Hudson RR. 1983. Properties of a neutral allele model with intragenic recombination. *Theor.*
1065 *Popul. Biol.* 23:183–201.

1066 Hudson RR, Kaplan NL. 1995. Deleterious background selection with recombination. *Genetics*
1067 141:1605–1617.

1068 Jarvis ED, Mirarab S, Aberer AJ, Li B, Houde P, Li C, Ho SYW, Faircloth BC, Nabholz B,
1069 Howard JT, et al. 2014. Whole-genome analyses resolve early branches in the tree of life of
1070 modern birds. *Science* 346:1320–1331.

1071 Jensen JD, Payseur BA, Stephan W, Aquadro CF, Lynch M, Charlesworth D, Charlesworth B.
1072 2019. The importance of the Neutral Theory in 1968 and 50 years on: A response to Kern
1073 and Hahn 2018. *Evolution* 73:111–114.

1074 Johri P, Aquadro CF, Beaumont M, Charlesworth B, Excoffier L, Eyre-Walker A, Keightley PD,
1075 Lynch M, McVean G, Payseur BA, Pfeifer SP, Stephan W, Jensen JD. 2021. Unpublished
1076 data, http://dx.doi.org/10.1101/2021.10.27.466171, last accessed November 25, 2021.

1077 Johri P, Charlesworth B, Jensen JD. 2020. Toward an Evolutionarily Appropriate Null Model:
1078 Jointly Inferring Demography and Purifying Selection. *Genetics* 215:173–192.

1079 Johri P, Riall K, Becher H, Excoffier L, Charlesworth B, Jensen JD. 2021. The Impact of
1080 Purifying and Background Selection on the Inference of Population History: Problems and
1081 Prospects. *Mol. Biol. Evol.* 38:2986–3003.

1082 Jónsson H, Sulem P, Arnadottir GA, Pálsson G, Eggertsson HP, Kristmundsdottir S, Zink F,
1083 Kehr B, Hjorleifsson KE, Jensson BÖ, et al. 2018. Multiple transmissions of de novo
1084 mutations in families. *Nat. Genet.* 50:1674–1680.

1085 Kaback D, Guacci V, Barber D, Mahon J. 1992. Chromosome size-dependent control of meiotic
1086 recombination. *Science* 256:228–232.

1087 Kartje ME, Jing P, Payseur BA. 2020. Weak Correlation between Nucleotide Variation and
1088 Recombination Rate across the House Mouse Genome. *Genome Biol. Evol.* 12:293–299.

1089 Kawakami T, Smeds L, Backström N, Husby A, Qvarnström A, Mugal CF, Olason P, Ellegren
1090 H. 2014. A high density linkage map enables a second generation collared flycatcher
1091 genome assembly and reveals the patterns of avian recombination rate variation and
1092 chromosomal evolution. *Molecular Ecology* 23:4035–4058.

1093 Kern AD, Hahn MW. 2018. The Neutral Theory in Light of Natural Selection. *Mol. Biol. Evol.*
1094 35:1366–1371.

1095 Kern AD, Schrider DR. 2016. Discoal: flexible coalescent simulations with selection.
1096 *Bioinformatics* 32:3839–3841.

1097 Kern AD, Schrider DR. 2018. diploS/HIC: An Updated Approach to Classifying Selective
1098 Sweeps. *G3* 8:1959–1970.

1099 Knowles LL. 2009. Statistical Phylogeography. *Annu. Rev. Ecol. Evol. Syst.* 40:593–612.

1100 Korunes KL, Noor MAF. 2017. Gene conversion and linkage: effects on genome evolution and
1101 speciation. *Mol. Ecol.* 26:351–364.

1102 Kuhn M. 2008. Building predictive models in R using the caret package. J. Stat. Softw. 28, 1–26.

1103 Langley CH, Stevens K, Cardeno C, Lee YCG, Schrider DR, Pool JE, Langley SA, Suarez C,
1104 Corbett-Detig RB, Kolaczkowski B, et al. 2012. Genomic variation in natural populations of
1105 Drosophila melanogaster. *Genetics* 192:533–598.

1106 Leaché AD, Harris RB, Rannala B, Yang Z. 2014. The influence of gene flow on species tree
1107 estimation: a simulation study. *Syst. Biol.* 63:17–30.

1108 Li G, Figueiró HV, Eizirik E, Murphy WJ. 2019. Recombination-Aware Phylogenomics Reveals
1109 the Structured Genomic Landscape of Hybridizing Cat Species. *Mol. Biol. Evol.* 36:2111–
1110 2126.

1111 Li H. 2011. A statistical framework for SNP calling, mutation discovery, association mapping
1112 and population genetical parameter estimation from sequencing data. *Bioinformatics*
1113 27:2987–2993.

1114 Li H, Durbin R. 2009. Fast and accurate short read alignment with Burrows–Wheeler transform.
1115 *Bioinformatics* 25:1754–1760.

1116 Li H, Ralph P. 2019. Local PCA Shows How the Effect of Population Structure Differs Along
1117 the Genome. *Genetics* 211:289–304.

1118 Luna LW, Ribas CC, Aleixo A. 2021. Genomic differentiation with gene flow in a widespread
1119 Amazonian floodplain specialist bird species. *J.*
1120 *Biogeogr.*:https://doi.org/10.1111/jbi.14257

1121 Lynch Alfaro JW, Boubli JP, Paim FP, Ribas CC, Silva MNF da, Messias MR, Röhe F, Mercês
1122 MP, Silva Júnior JS, Silva CR, et al. 2015. Biogeography of squirrel monkeys (genus
1123 Saimiri): South-central Amazon origin and rapid pan-Amazonian diversification of a
1124 lowland primate. *Mol. Phylogenet. Evol.* 82 Pt B:436–454.

1125 Mangin B, Siberchicot A, Nicolas S, Doligez A, This P, Cierco-Ayrolles C. 2012. Novel
1126 measures of linkage disequilibrium that correct the bias due to population structure and
1127 relatedness. *Heredity* 108:285–291.

1128 Manthey JD, Klicka J, Spellman GM. 2021. The genomic signature of allopatric speciation in a
1129 songbird is shaped by genome architecture (Aves: Certhia americana). *Genome Biol.*
1130 *Evol.*:http://dx.doi.org/10.1093/gbe/evab120

1131 Martin SH, Davey JW, Salazar C, Jiggins CD. 2019. Recombination rate variation shapes
1132 barriers to introgression across butterfly genomes. *PLoS Biol.* 17:e2006288.

1133 Martin SH, Van Belleghem SM. 2017. Exploring Evolutionary Relationships Across the Genome
1134 Using Topology Weighting. *Genetics* 206:429–438.

1135 Mather K. 1938. CROSSING-OVER. *Biological Reviews* 13:252–292

1136 McKenna A, Hanna M, Banks E, Sivachenko A, Cibulskis K, Kernytsky A, Garimella K,
1137 Altshuler D, Gabriel S, Daly M, et al. 2010. The Genome Analysis Toolkit: a MapReduce
1138 framework for analyzing next-generation DNA sequencing data. *Genome Res.* 20:1297–
1139 1303.

1140 McVicker G, Gordon D, Davis C, Green P. 2009. Widespread genomic signatures of natural
1141 selection in hominid evolution. *PLoS Genet.* 5:e1000471.

1142 Meunier J, Duret L. 2004. Recombination drives the evolution of GC-content in the human
1143 genome. *Mol. Biol. Evol.* 21:984–990.

1144 Mezmouk S, Dubreuil P, Bosio M, Décousset L, Charcosset A, Praud S, Mangin B. 2011. Effect
1145 of population structure corrections on the results of association mapping tests in complex
1146 maize diversity panels. *Theor. Appl. Genet.* 122:1149–1160.

1147 Mikkelsen EK, Weir JT. 2020. The genome of the Xingu scale-backed antbird (Willisornis vidua
1148 nigrigula) reveals lineage-specific adaptations. *Genomics* 112:4552–4560.

1149 Minh BQ, Schmidt HA, Chernomor O, Schrempf D, Woodhams MD, von Haeseler A, Lanfear
1150 R. 2020. IQ-TREE 2: New Models and Efficient Methods for Phylogenetic Inference in the
1151 Genomic Era. *Mol. Biol. Evol.* 37:1530–1534.

1152 Mořkovský L, Janoušek V, Reif J, Rídl J, Pačes J, Choleva L, Janko K, Nachman MW, Reifová
1153 R. 2018. Genomic islands of differentiation in two songbird species reveal candidate genes
1154 for hybrid female sterility. *Mol. Ecol.* 27:949–958.

1155 Musher LJ, Giakoumis M, Albert J, Del Rio G, Rego M, Thom G, Aleixo A, Ribas CC,

1156 Brumfield RT, Smith BT, Cracraft J. 2021. Unpublished data,
1157 https://www.biorxiv.org/content/10.1101/2021.11.15.468717v1, last accessed November
1158 25, 2021.

1159 Nachman MW, Payseur BA. 2012. Recombination rate variation and speciation: theoretical
1160 predictions and empirical results from rabbits and mice. *Philos. Trans. R. Soc. Lond. B Biol.*
1161 *Sci.* 367:409–421.

1162 Nguyen L-T, Schmidt HA, von Haeseler A, Minh BQ. 2015. IQ-TREE: A Fast and Effective
1163 Stochastic Algorithm for Estimating Maximum-Likelihood Phylogenies. *Molecular Biology*
1164 *and Evolution* 32:268–274.

1165 de Oliveira DP, de Carvalho VT, Hrbek T. 2016. Cryptic diversity in the lizard genus Plica
1166 (Squamata): phylogenetic diversity and Amazonian biogeography. *Zool. Scr.* 45:630–641.

1167 Ortiz EM. 2019. vcf2phylip v2.0: convert a VCF matrix into several matrix formats for
1168 phylogenetic analysis. Available from: https://zenodo.org/record/2540861

1169 Pavlidis P, Laurent S, Stephan W. 2010. msABC: a modification of Hudson's ms to facilitate
1170 multi-locus ABC analysis. *Mol. Ecol. Resour.* 10:723–727.

1171 Penz C, DeVries P, Tufto J, Lande R. 2015. Butterfly dispersal across Amazonia and its
1172 implication for biogeography. *Ecography* 38:410–418.

1173 Pessia E, Popa A, Mousset S, Rezvoy C, Duret L, Marais GAB. 2012. Evidence for widespread
1174 GC-biased gene conversion in eukaryotes. *Genome Biol. Evol.* 4:675–682.

1175 Pfeifer B, Wittelsbürger U, Ramos-Onsins SE, Lercher MJ. 2014. PopGenome: an efficient
1176 Swiss army knife for population genomic analyses in R. *Mol. Biol. Evol.* 31:1929–1936.

1177 Pouyet F, Aeschbacher S, Thiéry A, Excoffier L. 2018. Background selection and biased gene
1178 conversion affect more than 95% of the human genome and bias demographic inferences.
1179 *Elife* 7: http://dx.doi.org/10.7554/eLife.36317

1180 Rabiee M, Sayyari E, Mirarab S. 2019. Multi-allele species reconstruction using ASTRAL. *Mol.*
1181 *Phylogenet. Evol.* 130:286–296.

1182 Ribas CC, Aleixo A, Nogueira ACR, Miyaki CY, Cracraft J. 2012. A palaeobiogeographic
1183 model for biotic diversification within Amazonia over the past three million years. *Proc.*
1184 *Biol. Sci.* 279:681–689.

1185 Rousselle M, Mollion M, Nabholz B, Bataillon T, Galtier N. 2018. Overestimation of the
1186 adaptive substitution rate in fluctuating populations. *Biol. Lett.* 14:
1187 http://dx.doi.org/10.1098/rsbl.2018.0055

1188 Roux C, Fraïsse C, Castric V, Vekemans X, Pogson GH, Bierne N. 2014. Can we continue to
1189 neglect genomic variation in introgression rates when inferring the history of speciation? A
1190 case study in a Mytilus hybrid zone. *J. Evol. Biol.* 27:1662–1675.

1191 Schrider DR, Shanku AG, Kern AD. 2016. Effects of linked selective sweeps on demographic
1192 inference and model selection. *Genetics* 204:1207–1223.

1193 Schumer M, Xu C, Powell DL, Durvasula A, Skov L, Holland C, Blazier JC, Sankararaman S,
1194 Andolfatto P, Rosenthal GG, et al. 2018. Natural selection interacts with recombination to
1195 shape the evolution of hybrid genomes. *Science* 360:656–660.

1196 Seehausen O, Butlin RK, Keller I, Wagner CE, Boughman JW, Hohenlohe PA, Peichel CL,
1197 Saetre G-P, Bank C, Brännström A, et al. 2014. Genomics and the origin of species. *Nat.*
1198 *Rev. Genet.* 15:176–192.

1199 da Silva JMC, Rylands AB, da FONSECA GAB. 2005. The fate of the amazonian areas of
1200 endemism. *Conserv. Biol.* 19:689–694.

1201 Silva SM, Peterson AT, Carneiro L, Burlamaqui TCT, Ribas CC, Sousa-Neves T, Miranda LS,
1202 Fernandes AM, d'Horta FM, Araújo-Silva LE, et al. 2019. A dynamic continental moisture
1203 gradient drove Amazonian bird diversification. *Sci Adv* 5:eaat5752.

1204 Singhal S, Leffler EM, Sannareddy K, Turner I, Venn O, Hooper DM, Strand AI, Li Q, Raney B,
1205 Balakrishnan CN, et al. 2015. Stable recombination hotspots in birds. *Science* 350:928–932.

1206 Smith BT, McCormack JE, Cuervo AM, Hickerson MJ, Aleixo A, Cadena CD, Pérez-Emán J,
1207 Burney CW, Xie X, Harvey MG, et al. 2014. The drivers of tropical speciation. *Nature*
1208 515:406–409.

1209 Smith JM, Haigh J. 1974. The hitch-hiking effect of a favourable gene. *Genet. Res.* 23:23–35.

1210 Smith TCA, Arndt PF, Eyre-Walker A. 2018. Large scale variation in the rate of germ-line de
1211 novo mutation, base composition, divergence and diversity in humans. *PLoS Genet.*
1212 14:e1007254.

1213 Solís-Lemus C, Ané C. 2016. Inferring Phylogenetic Networks with Maximum Pseudolikelihood
1214 under Incomplete Lineage Sorting. *PLoS Genet.* 12:e1005896.

1215 Stankowski S, Chase MA, Fuiten AM, Rodrigues MF, Ralph PL, Streisfeld MA. 2019.
1216 Widespread selection and gene flow shape the genomic landscape during a radiation of
1217 monkeyflowers. *Plos Biology*: http://dx.doi.org/10.1101/342352

1218 Terhorst J, Kamm JA, Song YS. 2017. Robust and scalable inference of population history from
1219 hundreds of unphased whole genomes. *Nat. Genet.* 49:303–309.

1220 Tigano A, Khan R, Omer AD, Weisz D, Dudchenko O, Multani AS, Pathak S, Behringer RR,
1221 Aiden EL, Fisher H, MacManes MD. 2021. Unpublished data,
1222 https://www.biorxiv.org/content/10.1101/2021.01.15.426870v1, last accessed November
1223 25, 2021.

1224 Thom G, Aleixo A. 2015. Cryptic speciation in the white-shouldered antshrike (Thamnophilus
1225 aethiops, Aves – Thamnophilidae): The tale of a transcontinental radiation across rivers in

lowland Amazonia and the northeastern Atlantic Forest. Molecular Phylogenetics and Evolution 82:95–110.

Thom G, Xue AT, Sawakuchi AO, Ribas CC, Hickerson MJ, Aleixo A, Miyaki C. 2020. Quaternary climate changes as speciation drivers in the Amazon floodplains. Sci Adv 6:eaax4718.

Van Belleghem SM, Baquero M, Papa R, Salazar C, McMillan WO, Counterman BA, Jiggins CD, Martin SH. 2018. Patterns of Z chromosome divergence among Heliconius species highlight the importance of historical demography. *Mol. Ecol.* 27:3852–3872.

Van Doren BM, Campagna L, Helm B, Illera JC, Lovette IJ, Liedvogel M. 2017. Correlated patterns of genetic diversity and differentiation across an avian family. *Mol. Ecol.* 26:3982–3997.

Vijay N, Weissensteiner M, Burri R, Kawakami T, Ellegren H, Wolf JBW. 2017. Genomewide patterns of variation in genetic diversity are shared among populations, species and higher-order taxa. *Mol. Ecol.* 26:4284–4295.

Waterhouse RM, Seppey M, Simão FA, Manni M, Ioannidis P, Klioutchnikov G, Kriventseva EV, Zdobnov EM. 2018. BUSCO Applications from Quality Assessments to Gene Prediction and Phylogenomics. *Mol. Biol. Evol.* 35:543–548.

Watterson GA. 1975. On the number of segregating sites in genetical models without recombination. *Theor. Popul. Biol.* 7:256–276.

Wayne ML, Simonsen KL. 1998. Statistical tests of neutrality in the age of weak selection. *Trends Ecol. Evol.* 13:236–240.

Weir JT, Faccio MS, Pulido-Santacruz P, Barrera-Guzmán AO, Aleixo A. 2015. Hybridization in headwater regions, and the role of rivers as drivers of speciation in Amazonian birds. *Evolution* 69:1823–1834.

Wen D, Yu Y, Zhu J, Nakhleh L. 2018. Inferring Phylogenetic Networks Using PhyloNet. *Syst. Biol.* 67:735–740.

Wolf JBW, Ellegren H. 2017. Making sense of genomic islands of differentiation in light of speciation. *Nat. Rev. Genet.* 18:87–100.

Wu TD, Watanabe CK. 2005. GMAP: a genomic mapping and alignment program for mRNA and EST sequences. *Bioinformatics* 21:1859–1875.

Zeng K. 2013. A coalescent model of background selection with recombination, demography and variation in selection coefficients. *Heredity* 110:363–371.

Zhang C, Rabiee M, Sayyari E, Mirarab S. 2018. ASTRAL-III: polynomial time species tree reconstruction from partially resolved gene trees. *BMC Bioinformatics* 19:153.

Zhang G, Li C, Li Q, Li B, Larkin DM, Lee C, Storz JF, Antunes A, Greenwold MJ, Meredith RW, et al. 2014. Comparative genomics reveals insights into avian genome evolution and adaptation. *Science* 346:1311–1320.

Zheng X, Levine D, Shen J, Gogarten SM, Laurie C, Weir BS. 2012. A high-performance computing toolset for relatedness and principal component analysis of SNP data. *Bioinformatics* 28:3326–3328.